Accepted manuscript version
J. Phys. Chem. B, volumen *117*, pages 14599−14614 (2013)
DOI for the Published journal article (PJA): 10.1021/jp405121s

Conformational Preference and Chiroptical Response of Carbohydrates D-ribose and 2-deoxy-D-ribose in Aqueous and Solid Phases

María Mar Quesada-Moreno,[†] Luis Miguel Azofra,[‡] Juan Ramón Avilés-Moreno,[†] Ibon Alkorta,*[,‡] José Elguero[‡] and Juan Jesús López-González.*[,†]

[†]Department of Physical and Analytical Chemistry, University of Jaén, Campus Las Lagunillas, E-23071 Jaén, Spain.

[‡]Instituto de Química Médica (C.S.I.C.), Juan de la Cierva, 3, E-28006 Madrid, Spain.

ABSTRACT: This work targets the structural preferences of D-ribose and 2-deoxy-D-ribose in water solution and solid phase. A theoretical DFT (B3LYP and M06-2X) and MP2 study has been undertaken considering the five possible configurations (open-chain, α-furanose, β-furanose, α-pyranose and β-pyranose) of these two carbohydrates with a comparison of the solvent treatment using only a continuum solvation model (PCM) and the PCM plus one explicit water molecule. In addition, experimental vibrational studies using both non-chiroptical (IR-Raman) and chiroptical (VCD) techniques have been carried out. The theoretical and experimental results show that α- and β-pyranose forms are the dominant configurations for both compounds. Moreover, it has been found that 2-deoxy-D-ribose presents a non-negligible percentage of open-chain forms in aqueous solution, while in solid phase this configuration is absent.

KEYWORDS: conformational analysis; chirality; IR; Raman; VCD; DFT; MP2; PCM

INTRODUCTION

Carbohydrates of general formula $C_nH_{2n}O_n$ with $n \geq 2$ (the deoxy derivatives have O_{n-1} oxygen atoms) are the most abundant organic compounds on earth by mass, with a string of relevant functions as energy storage, metabolic intermediates and structural building blocks. Sugars with $n \geq 5$ are present in several forms of life, building up most of the bioorganic matter.[1-3] D-ribose and 2-deoxy-D-ribose are constituents of the nucleic acids RNA and DNA, respectively, and for this reason they are so relevant in biochemistry. The structure of D-ribose and 2-deoxy-D-ribose differs by the presence/absence of a hydroxyl group on C2 (Figure 1). Their interactions with water are very important because they affect the stabilities of native configurations of RNA and DNA.[4] Due to their importance in nucleic acids and due to the fact that they are in the human body surrounded by water, the study of the structures of these compounds in water is of considerable interest.

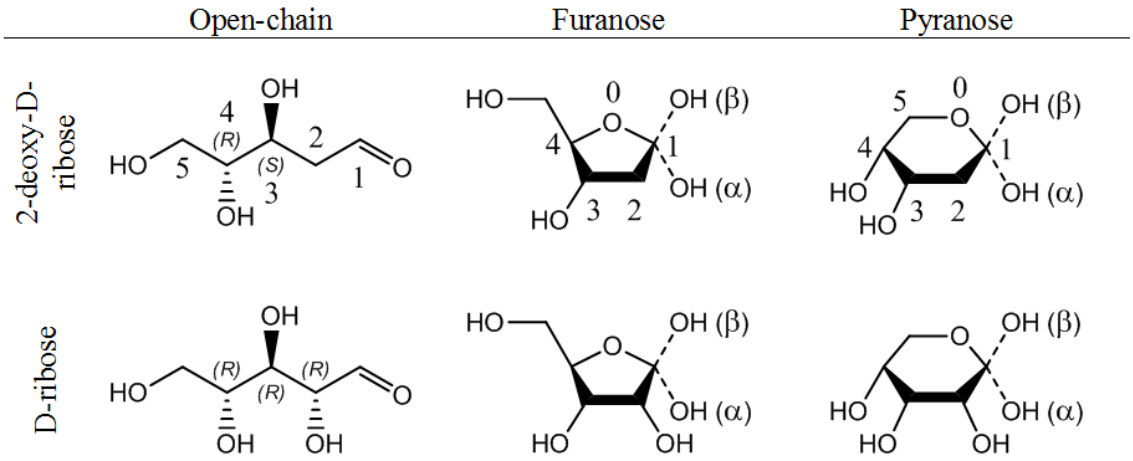

Figure 1. Left to right and top to bottom: open-chain, furanose and pyranose (α- and β-) configurations of 2-deoxy-D-ribose and D-ribose. The absolute configuration of the stereogenic centers is indicated in the linear forms. The numbering of 2-deoxy-D-ribose structures (extends to D-ribose) corresponds to the IUPAC recommendation.

D-ribose and 2-deoxy-D-ribose can exist in five forms, *i.e.*, one open-chain, two with five-membered rings, α- and β-furanoses, and two with six-membered rings, α- and β-pyranoses (Figure 1).[5] Ribose is usually described as furanose anomers, predominant in ribonucleosides, RNA, ATP, and other biochemical derivatives. The

conformational landscape and the flexibility of many carbohydrates have been analyzed by DFT and *ab initio* methods.[1,2,6-12] It is noteworthy that there is a good amount of structural data for D-ribose, but little to none for the isolated 2-deoxy-D-ribose. These statements will be discussed in the following paragraph. A theoretical study of the conformational profile of the methyl β-D-2-deoxyribofuranoside and methyl β-D-ribofuranoside was carried out using DFT methods and the influence of the conformation on the nuclear chemical shifts was analyzed.[13]

We have found some papers about structural studies of D-ribose and 2-deoxy-D-ribose. Concerning D-ribose, Jalbout *et al.* reported a computational analysis of the isolated β-furanose form of D-ribose.[14] Cocinero *et al.*[3] studied D-ribose in gas phase with a combination of quantum chemical calculations and FT-MW (Fourier-transform microwave) spectroscopy. They concluded that the α- and β-pyranose forms in this carbohydrate are more stable than the furanose forms. These authors were able to characterize six structures of α- and β-pyranose in an energy range of 2 kJ mol^{-1},[3] which indicates the conformational complexity of this carbohydrate. Moreover, Angyal concluded that 58% of β-anomers is in the pyranose form and 13% of β-anomers is in the furanose form in solution by the use of NMR spectroscopy.[15] Mathlouthi *et al.*[16] analyzed the IR and Raman spectra of D-ribose and 2-deoxy-D-ribose in aqueous solution. They concluded that D-ribose was present in 76% pyranose and 24% furanose forms, though they do not report percentages for 2-deoxy-D-ribose. Yaylayan *et al.*[17] studied the enolization and carbonyl group migration of selected aldoses and ketoses with the use of IR spectroscopy. They analyzed these species in D_2O as a function of concentration and temperature, between 30 and 80 ºC, and they observed two relevant bands for these two carbohydrates. For D-ribose, the first one at 1722 cm^{-1}, assigned to the C=O stretching of the carbonyl group, and the second one at 1646 cm^{-1}, which corresponded to the C=C stretching of the enediol group. The enediol species were formed as a result of an enolization of acyclic aldehyde and keto forms of the carbohydrates. The ratio of intensities of enediol to carbonyl absorption bands decreases with temperature and increases with concentration. Šišak *et al.*[18] studied the structure of D-ribose in solid phase using both NMR spectroscopy and X-ray diffraction techniques. The molecules in the crystal presented the pyranose ring structure, with a β/α ratio of 2:1 and 3:1 according to the analysis of the powder and single-crystal, respectively. Moreover, the melted and newly recrystallized sample showed a β/α ratio of 2.5:1. The

authors pointed out that the reliability of the calculated β/α ratios is difficult to estimate, as the ratios were determined from different experiments.

For 2-deoxy-D-ribose, Lemieux *et al.*[19] studied its mutarotation in H_2O and D_2O solutions by ^1H NMR spectroscopy and OR (optical rotatory) measurements. They concluded that this carbohydrate rearranges, giving an equilibrium mixture which contains the α- and β-pyranose and furanose anomers in the approximate percentage ratios of 43(βp):42(αp):10(βf):5(αf) at 0 ºC and 30(βp):30(αp):18(βf):22(αf) at 90 ºC. For 2-deoxy-D-ribose, Yaylayan *et al.*[17] reported that the first band was observed at 1715 cm^{-1} and the second one was absent.

The chiral response of the 2-deoxy-D-ribose has not been studied yet, however, some studies exist in the case of the D-ribose. Thus, Tummalapalli *et al.*[20] recorded the IR and VCD spectra of simple carbohydrates, including D-ribose, in DMSO-d_6 solutions in the 1650-800 cm^{-1} region. They eliminated the presence of artifacts in the VCD spectrum equilibrating a given enantiomer with H_2O or D_2O and lyophilizing the equilibrated solution. The authors point out the difficulty of the identification of all the structures participating in the VCD features. Besides, Bose *et al.*[21] analysed the IR and VCD spectra of the D-ribose and several monosaccharides in DMSO-d_6 solutions in the 1500-1180 cm^{-1} region. The authors conclude for D-ribose, among other monosaccharides, that this carbohydrate exits in both pyranose and furanose forms. The VCD spectra of other carbohydrates have been analyzed by Polavarapu and co-workers,[22] using films formed from aqueous solutions of D-glucose or D-allose in the 2000-900 cm^{-1} region while Monde and co-workers[23] reported VCD studies of some disaccharides in the CH vibrational region. In addition, Wen *et al.*[24] recorded the ROA spectra of D-ribose and of 14 monosaccharides in aqueous solution in the 1600-600 cm^{-1} spectral region. For D-ribose, they concluded that it exists probably in both pyranose and furanose forms, but a further analysis in the region below 700 cm^{-1} would be necessary to verify this point. All these results are empiric conclusions and they have been carried out without the help of the calculations.

Šišak *et al.*[18] pointed out that in the past, most of the modern chemistry text books and handbooks showed the molecule of D-ribose in the β-furanose form, as present in biochemically important ribose derivatives. But it has been known from NMR spectroscopy and X-ray diffraction techniques that the molecules of D-ribose in the crystal present the pyranose ring structure. In addition, it has been shown from NMR

observations that D-ribose exists in aqueous solutions as a mixture of α- and β-pyranoses and α- and β-furanoses with a predominance of the β-pyranose form. Moreover, Yaylayan also found the presence of enediol in the open-chain structures, as well as the predominance of pyranoses.[17] All the studies in solution for both monosaccharides agree on: i) the major presence of pyranoses; ii) the minor presence of furanoses; and iii) a negligible amount of open-chain structures (in both forms derived from the keto-enol tautomerism). Lemieux *et al.*[19] agree with a major proportion of pyranose forms of D-ribose in aqueous solutions but did not find evidence substantiating the presence of open-chain forms. At this point, we could summarize that it is clear that in solution, pyranose forms predominate over furanose ones and that there remains a controversy about the presence of open-chain forms and about the α/β ratio of pyranose forms.

In order to clarify both the configurational preference and the conformational landscape of D-ribose and 2-deoxy-D-ribose in aqueous solution, in the present work, we carried out a detailed study of the structures of these two carbohydrates by quantum chemical calculations (thousands of structures have been modeled) coupled with chiral sensitive (VCD) and non-sensitive (IR and Raman) vibrational spectroscopies. The treatment of the solvent (water) has been modelized using only solvent continuum models (PCM) and PCM plus an explicit water molecule. In addition, we have also analyzed the experimental spectroscopic properties of these carbohydrates in solid phase.

METHODS

Theoretical calculations.

The conformational searches were conducted in two steps. In the first one, a large number of initial structures were chosen based on the different rotatable bonds (linear and cyclic forms) and the ring conformations (only in cyclic forms). Thus, in the open-chain configurations of 2-deoxy-D-ribose and D-ribose there are seven and eight rotatable bonds, respectively. For each rotatable bond, three possibilities have been considered: gauche, gauche' and trans (*g*, *g*' and *t*) giving 2187 (3^7) and 6561 (3^8) initial structures, respectively. In the case of the furanose forms, twenty ring conformations

(ten envelope and ten twist) were combined with the four and five rotatable bonds for α/β-2-deoxy-D-ribofuranose and α/β-D-ribofuranose, respectively. Considering the three mentioned conformations (*g*, *g*', and *t*) for the rotatable bonds, the total number of initial conformations is 1620 ($20 \cdot 3^4$) and 4860 ($20 \cdot 3^5$), respectively. Finally, for the pyranose structures, thirty-eight ring conformations (two chair, twelve half-chair, six skew, six boat and twelve envelope) were combined with three and four rotatable bonds for α/β-2-deoxy-D-ribopyranose and α/β-D-ribopyranose, which corresponds to 1026 ($38 \cdot 3^3$) and 3078 ($38 \cdot 3^4$) initial structures, respectively. All these structures were optimized with the Becke,[25] three-parameter, Lee-Yang-Parr[26] density functional (B3LYP) and Pople's basis set 6-31G,[27] taken into account the solvent effect through the use of the Polarizable Continuum Model (PCM)[28] with the use of a dielectric constant $\varepsilon = 78.36$, corresponding to water (PCM-water). Structures with a geometrical root mean square less than 0.05 Å and electronic differences less than 0.1 kJ mol^{-1} were considered to be identical; duplicate structures are removed.[1] The resulting geometries were optimized in a second step with two different functionals: on the one hand, the M06-2X,[29] and on the other hand, the B3LYP[25,26] hybrid functionals, and in both cases with the Pople's basis set 6-311++G(d,p)[27] which includes diffuse and polarization functions for heavy and light atoms. The solvent effect has been simulated with the PCM-water method,[30-34] including, in this case, the solute-solvent dispersion interaction energy, the solute-solvent repulsion interaction energy and the solute cavitation energy. All these structures were again compared to remove the repeated ones. Frequency calculations were carried out in order to confirm that the final structures correspond to real minima and to obtain the value of the Zero Point Energy (ZPE). The electronic energies have been corrected with the ZPE. In the most stable conformations, MP2(full)/6-311++G(3df,2p)//M06-2X/6-311++G(d,p) single point calculations[35-38] in PCM-water were performed to obtain more accurate energy values.

Finally, for each one of the most stable minima obtained at the M062X/6-311++G(d,p) computational level plus PCM, an explicit treatment of the solvent has been made by introducing one water molecule in several positions, pointing to each acidic and basic centers, that is, acting the water molecule as hydrogen bond acceptor (HBA) or donor (HBD), respectively. A total number of 701 geometries have been optimized for both carbohydrates using this methodology. The final number of non-redundant optimized structures was 229 for D-ribose and 144 for 2-deoxy-D-ribose.

All the DFT and MP2-calculations were carried out with the GAUSSIAN09 package.[39] The ring puckering analysis methodology developed by Cremer and Pople[40] was applied in order to characterize the pseudorotation parameters (P, θ, ϕ), which overlaid on the Altona-Sundaralingam wheel-sphere,[41] gives the type ring conformation, and the Q amplitude, *i.e.*, how much the ring is distorted with respect to the planar case. For this purpose, the RING96[40,42] and some in-house developed programs were employed.[1]

The electron density of the systems was analyzed within Atoms in Molecules (AIM) methodology[43,44] with the MORPHY[45-47] and AIMAll[48] programs. On the basis of this methodology, all the interactions (covalent and weak interactions) were characterized by the presence of a bond critical point (BCP) and the corresponding bond path linking the two interacting nuclear attractors. The values of the electron density and its Laplacian at the BCP allow to classify the contacts as covalent or non-covalent.[43,49,50] The Natural Bond Orbital (NBO)[51] theory was also applied for the orbital characterization of the weak interactions. These calculations were carried out with the NBO3.1 facilities.[52] Finally, harmonic IR, Raman and VCD calculations were computed.

Experimental Section.

All the experimental techniques employed in this work belong to Scientific Central Services (CICT) of the University of Jaén.[53]

a) Non-chiroptical vibrational spectroscopies (IR and Raman): The D-ribose and 2-deoxy-D-ribose were purchased from Sigma–Aldrich and used without further purification. IR and Raman spectra of D_2O and H_2O solutions (4 M) were registered.

A FT-IR 4100 JASCO spectrometer, equipped with a Globar source, a DGTS detector and KBr optics, was used to record the IR spectra with the ATR accessory for the solid (powder) and liquid samples. The IR spectra were recorded in the 4000-500 cm^{-1} range, with 300 scans and a resolution of 1 cm^{-1} and 4 cm^{-1} for the solid (powder) and liquid samples, respectively.

The Raman spectra of D-ribose and 2-deoxy-D-ribose were recorded using a BRUKER MultiRAM Stand Alone FT-Raman Spectrometer, equipped with a Nd:YAG laser (excitation line at 1064 nm) and a Ge detector cooled at liquid nitrogen temperature. The spectra of the solid samples (powder) were measured using a standard

solid support with a resolution of 1 cm^{-1} and 200 scans. The spectra of the solutions were measured using standard liquid cells, with 300 scans and a resolution of 8 cm^{-1}. All the spectra were recorded in the 4000-100 cm^{-1} spectral range.

b) Chiroptical vibrational spectroscopy (VCD). The VCD spectra of D-ribose and 2-deoxy-D-ribose in 4M D_2O and H_2O solutions, in film and in fluorolube and nujol mulls were recorded using a JASCO FVS-4000 FTIR spectrometer, equipped with InSb (4000-1900 cm^{-1}) and MCT (2000-900 cm^{-1}) detectors. To record the film spectra, more diluted solutions were used to get the optimum absorbance range for the VCD measurement of the sample.

The solvent was evaporated using NaCl "Real Crystal IR Sample Cards"[54] in order to get very thin films. A few milligrams of the two samples were mixed with fluorolube or nujol mineral oils in order to get suitable mulls. Special attention is needed when working with solid samples in circular dichroism spectroscopy.[55-57] In fact, we have measured the mulls in several positions by rotating the sample around both the beam propagation axes (90º and 180º) and that perpendicular to it (180º) with the purpose to get the true VCD peaks and to be sure on the absence of artifacts in the recorded VCD spectra.[55] The film spectra were recorded using a KCl support, with a resolution of 4-8 cm^{-1} and 14000-28000 scans in blocks of 2000 scans. The remaining spectra were recorded using a standard cell equipped with BaF_2 windows, with a resolution of 4-8 cm^{-1}, path lengths of 6 microns (for solution spectra) and 2000-16000 scans in blocks of 2000 scans. Concerning the baseline correction, we have subtracted the D_2O, H_2O, KCl support, nujol and/or fluorolube signals to the VCD spectra.

RESULTS AND DISCUSSION

This section has been divided in four parts: the first one reports the theoretical study of the conformational landscape of 2-deoxy-D-ribose and D-ribose in aqueous solution models using only PCM and PCM plus an explicit water molecule. The second part describes the AIM and NBO analysis of the intramolecular weak interactions present in these compounds. The part three reports the experimental study of 2-deoxy-D-ribose and D-ribose by non-chiroptical vibrational IR and Raman spectroscopies. Finally, the fourth part describes the chiroptical vibrational response using VCD spectroscopy. Along the description of the results the next abbreviations will be employed: dDR, DR,

dDRαf, dDRβf, DRαf, DRβf, dDRαp, dDRβp, DRαp and DRβp, which refer to open-chain 2-deoxy-D-ribose, open-chain D-ribose, α-2-deoxy-D-ribofuranose, β-2-deoxy-D-ribofuranose, α-D-ribofuranose, β-D-ribofuranose, α-2-deoxy-D-ribopyranose, β-2-deoxy-D-ribopyranose, α-D-ribopyranose and β-D-ribopyranose, respectively.

1.- Configurational preference and conformational landscape of 2-deoxy-D-ribose and D-ribose in aqueous solution.

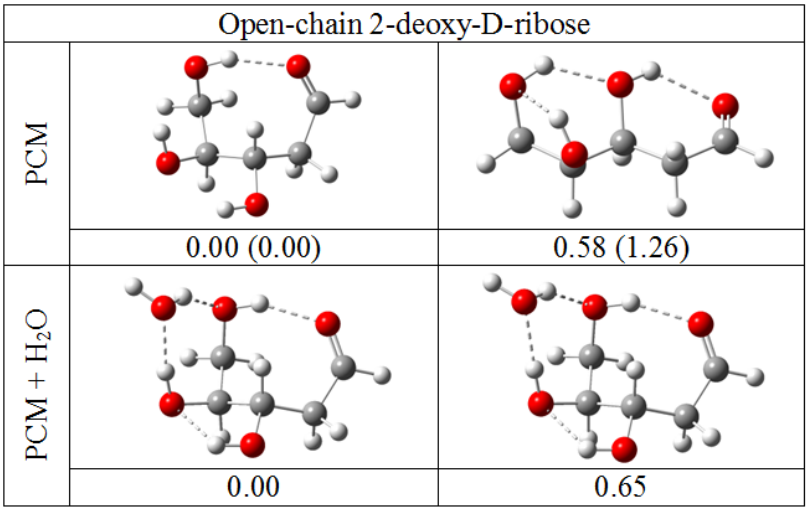

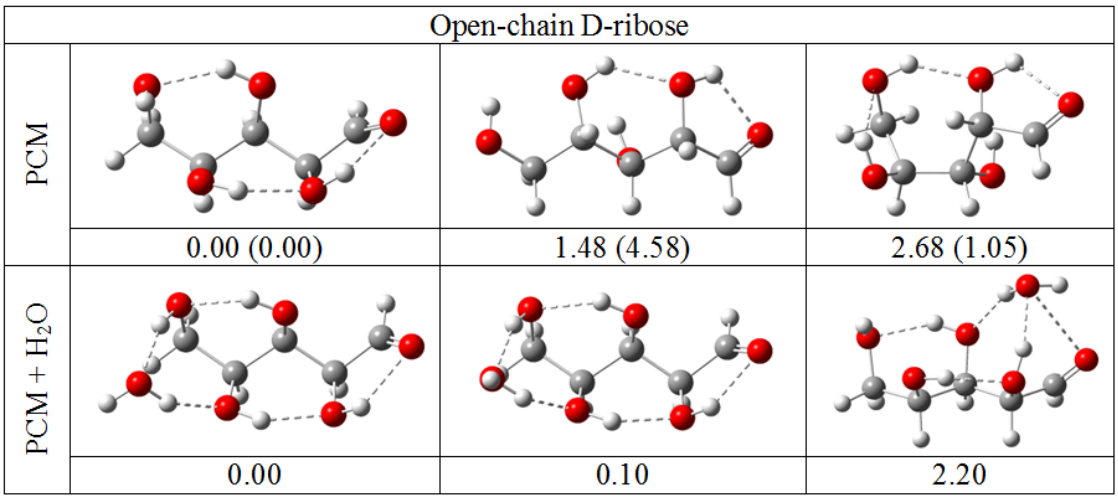

Figure 2. The most stable conformers (less than 3 kJ mol^{-1}) of the open-chain forms of 2-deoxy-D-ribose and D-ribose in PCM and PCM plus an explicit water molecule calculated at the M06-2X/6-311++G(d,p) computational level. Relative energies [MP2(full) results in parenthesis] are in kJ mol^{-1}. The dashed lines indicate the non-covalent interactions obtained in the AIM analysis.

α-2-deoxy-D-ribopyranose						
PCM	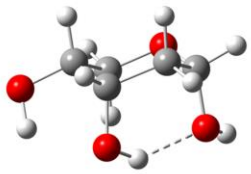		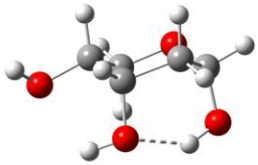		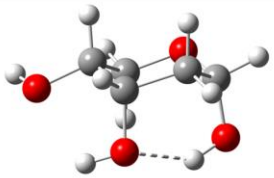	
	0.00 (0.00)		1.56 (1.28)		1.75 (1.30)	
	$^4C_1$	Q=0.548	$^4C_1$	Q=0.559	$^4C_1$	Q=0.562
PCM + H_2O	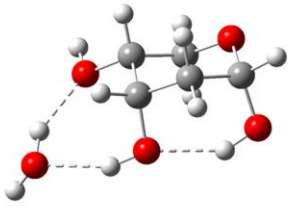		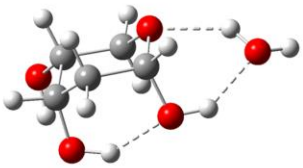		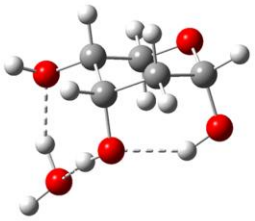	
	0.00		0.41		2.37	
	$^4C_1$	Q=0.575	$^4C_1$	Q=0.555	$^4C_1$	Q=0.572

β-2-deoxy-D-ribopyranose						
PCM	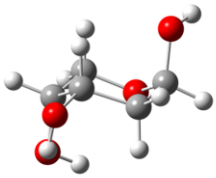		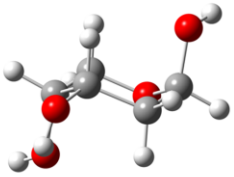		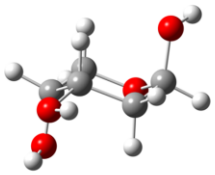	
	0.00 (0.00)		2.66 (4.06)		2.73 (3.61)	
	$^1C_4$	Q=0.566	$^1C_4$	Q=0.551	$^1C_4$	Q=0.552
	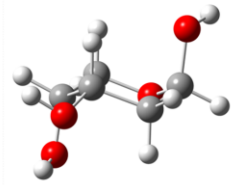					
	2.90 (2.76)					
	$^1C_4$	Q=0.549				
PCM + H_2O	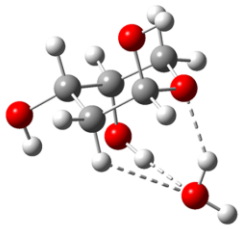					
	0.00					
	$^1C_4$	Q=0.554				

α-D-ribopyranose			
PCM	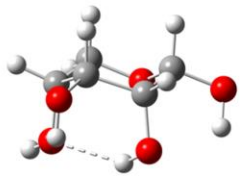	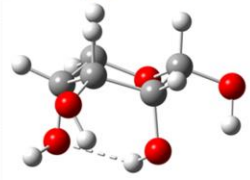	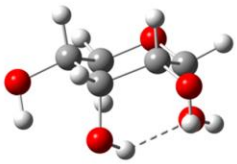
	0.00 (1.33)	0.09 (0.00)	1.41 (4.95)
	$^1C_4$ Q=0.569	$^1C_4$ Q=0.566	$^4C_1$ Q=0.553
	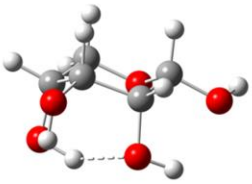	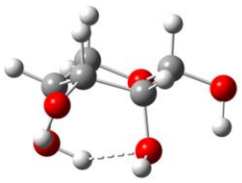	
	1.48 (4.38)	1.89 (2.37)	
	$^1C_4$ Q=0.571	$^1C_4$ Q=0.568	
PCM + H_2O	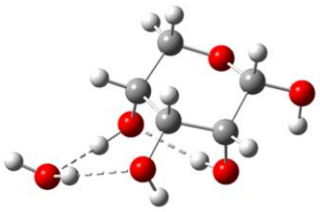	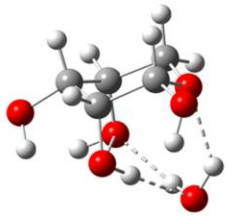	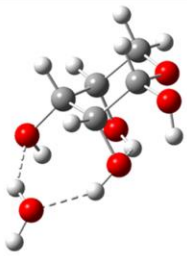
	0.00	0.24	0.65
	$^1C_4$ Q=0.574	$^1C_4$ Q=0.550	$^1C_4$ Q=0.574
	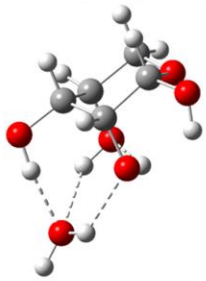	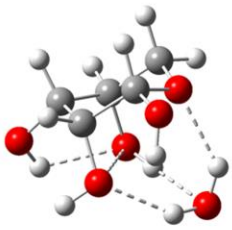	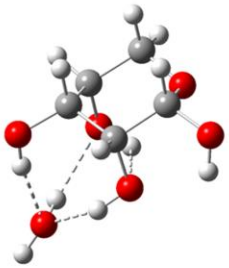
	1.79	1.82	2.18
	$^1C_4$ Q=0.585	$^1C_4$ Q=0.547	$^1C_4$ Q=0.589
	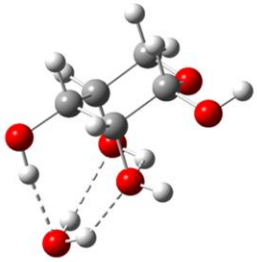	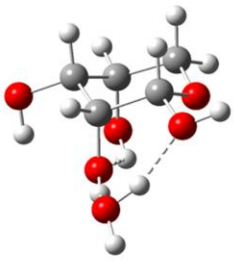	
	2.57	2.84	
	$^1C_4$ Q=0.586	$^1C_4$ Q=0.584	

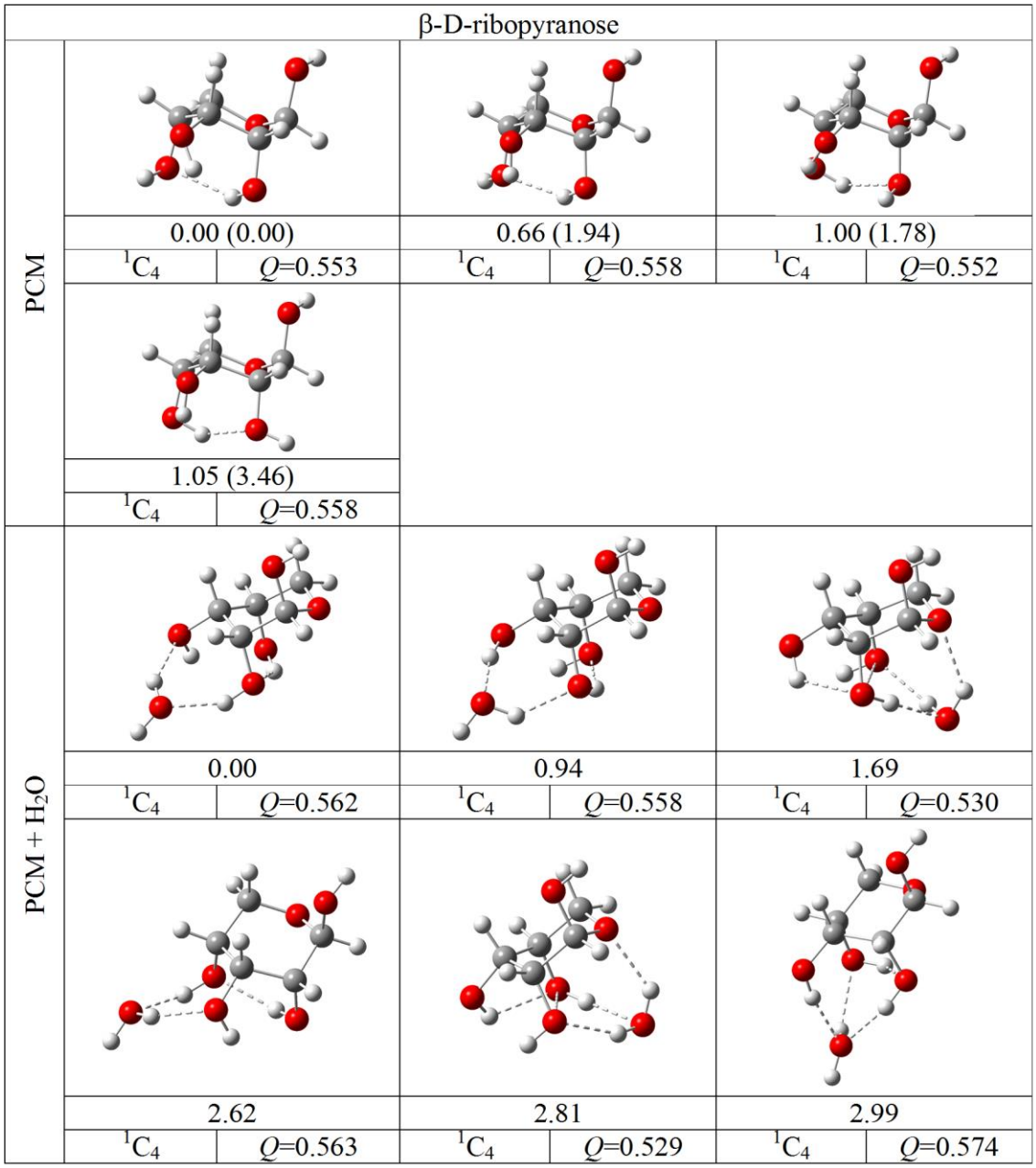

Figure 3. The most stable conformers (less than 3 kJ mol^{-1}) of the pyranose (α- and β-) forms of 2-deoxy-D-ribose and D-ribose in PCM and PCM plus an explicit water molecule calculated at the M06-2X/6-311++G(d,p) computational level. Relative energies [MP2(full) results in parenthesis] are in kJ mol^{-1}. Both the ring conformation[a] and the *Q* parameter in Å are included. The dashed lines indicate the non-covalent interactions obtained in the AIM analysis.

[a]C=chair, H=half-chair, S=skew, B=boat and E=envelope. Superscript at the left refers to *endo* face. Subscript at the right refers to *exo* face.

Table 1. Conformational search summary.

				PCM/M06-2X		PCM+H2O/M06-2X	
Struc.	Initial	Screen[a]	Final[b]	<10 kJ mol^{-1}	<5 kJ mol^{-1}	<10 kJ mol^{-1}	<5 kJ mol^{-1}
dDR	2187	1070	1005	21	3	9	4
DR	6561	2200	1916	27	6	8	3
dDRαf	1620	149	117	27	8	16	4
dDRβf	1620	168	148	22	11	15	6
DRαf	4860	238	201	40	13	24	13
DRβf	4860	311	266	25	13	18	11
dDRαp	1026	121	105	5	4	11	4
dDRβp	1026	153	146	15	4	14	4
DRαp	3078	243	188	21	8	24	9
DRβp	3078	310	272	14	5	18	9

[a]1st screening at B3LYP/6-31G computational level.

[b]2nd screening with the employment of the 6-311++G(d,p) basis set.

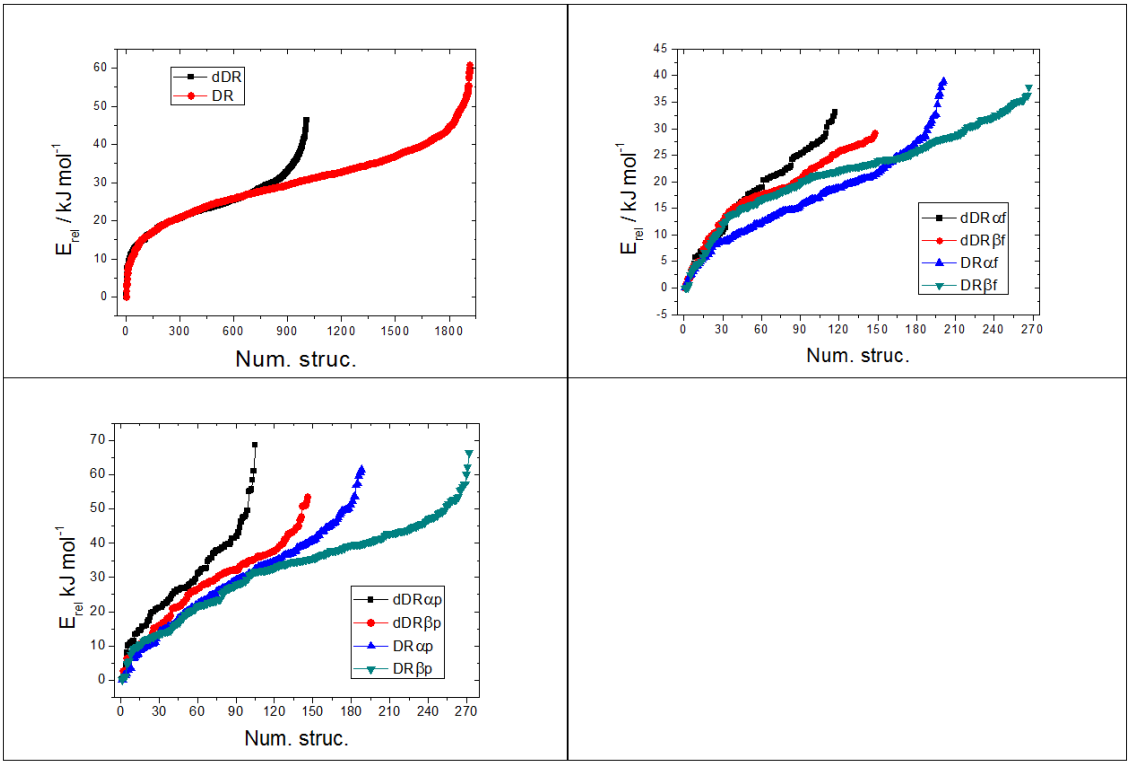

Figure 4. Left to right and top to bottom: variation of all open-chain, furanose and pyranose conformations of 2-deoxy-D-ribose and D-ribose according to the M06-2X/6-311++G(d,p) relative energy to their respective global minima.

A total of 1005 and 1916 unique minima were found for the open-chain forms of 2-deoxy-D-ribose and D-ribose, respectively, at M06-2X/6-311++G(d,p) computational level. In the furanose cases, 117, 148, 201 and 266 unique minima were obtained for α-2-deoxy-D-ribofuranose, β-2-deoxy-D-ribofuranose, α-D-ribofuranose and β-D-ribofuranose, respectively. Finally, the number of unique minima for the pyranose

forms is 105, 146, 188 and 272 for α-2-deoxy-D-ribopyranose, β-2-deoxy-D-ribopyranose, α-D-ribopyranose and β-D-ribopyranose, in each case (see Table 1). As can be seen, the number of minima obtained in the cyclic conformations is much smaller than in the open-chain forms, due to the restrictions imposed by the ring. A similar number of minima is obtained when the B3LYP/6-311++G(d,p) computational level is used, except for the open-chain D-ribose where only 1664 minima are found, which is about 250 less than those obtained in the M06-2X/6-311++G(d,p) calculations (see Figure 4).

Figures 2 and 3 show the most stable conformers (less than 3 kJ mol^{-1}) of the open-chain and pyranose (α- and β-) forms of 2-deoxy-D-ribose and D-ribose in PCM and PCM plus an explicit water molecule calculated at the M06-2X/6-311++G(d,p) computational level. We can find this information for furanose (α- and β-) forms in the Supplementary Information (Figure S1). In addition, the most stable conformers (less than 5 kJ mol^{-1}) of the five forms of 2-deoxy-D-ribose and D-ribose in PCM-water calculated at the M06-2X/6-311++G(d,p) computational level are also gathered in the Supplementary Information (see Figures S2, S3 and S4).

The most stable minimum of the open-chain 2-deoxy-D-ribose exhibits a compact structure in the carbon skeleton, while the opposite happens in the second and third more stable minima. In the open-chain D-ribose, all the minima with a relative energy less than 5 kJ mol^{-1}, present at least one of their D_{CCCC} with an *s-trans* configuration.

$^{2}T_{1}$ and ^{2}E conformations are found in the most stable minima of the α-2-deoxy-D-ribofuranose, which are in the same Altona-Sundaralingam wheel zone. These ones favor the hydrogen bond (HB) formation between the hydroxyl groups on the *exo* face. In half of the minima, the hydroxymethyl group points into the ring with the formation of a HB between its oxygen atom and the *endo* hydrogen atom bonded to C2. In β-2-deoxy-D-ribofuranose, ^{4}E predominates as ring conformation of the most stable minima with the appearance of an explicit O···C2 interaction, where the oxygen atom is part of the hydroxymethyl moiety. In addition, four $^{1}T_{2}$ conformations are found with relative energies between 4.2 and 5.0 kJ mol^{-1}. The $^{2}T_{1}$-^{2}E and E_{2}-$^{1}T_{2}$ conformations are found in the most stable minima of the α- and β-D-ribofuranose, respectively. In some cases, a HB between the hydroxymethyl group and the *endo* hydrogen atom of C2 is found as in the case of the α-2-deoxy-D-ribofuranose previously mentioned. Other low minima conformations found are the $^{3}T_{4}$ and the ^{4}E-$^{4}T_{3}$ in the α- and β-D-ribofuranose, with

relative energies between 3.57 and 4.98 kJ mol^{-1}, and 2.79 and 4.71 kJ mol^{-1}, respectively.

Finally, regarding pyranose forms, the most stable minimum energy structures of α-2-deoxy-D-ribopyranose present a $^4C_1$ ring conformation, whereas that for β-2-deoxy-D-ribopyranose, it is $^1C_4$. For β-2-deoxy-D-ribopyranose the $^4C_1$ ring conformation appears in the fifth ranking position, with a relative energy of 6.39 kJ mol^{-1} (0.06% of the Boltzmann population taking into account all the conformers). In α- and β-D-ribopyranose the $^1C_4$ conformations are the most stable in both cases. It is very important to highlight that in all the most stable pyranose minima, only chair conformations are present with different orientations of the hydroxyl groups.

Table 2. Relative energy in kJ mol^{-1} and Boltzmann population in percentage for the most stable minima (restricted for conformers with energies less than 5 kJ mol^{-1})[a] of 2-deoxy-D-ribose and D-ribose (open-chain, furanose and pyranose forms) at the M06-2X/6-311++G(d,p) and MP2(full)/6-311++G(3df,2p)//M06-2X/6-311++G(d,p) computational levels (T = 298.16 K).

	PCM M06-2X/6-311++G(d,p)		**PCM MP2(full)/ 6-311++(3df,2p)//M06-2X/6-311++G(d,p)//**		**PCM + explicit H_2O M06-2X/6-311++G(d,p)**		
Open-chain 2-deoxy-D-ribose							
Struc.	ΔE_0	% Pop.	ΔE_0	% Pop.	Struc.	ΔE_0	% Pop.
dDR01	0.00	50.6	0.00	59.6	dDR-w01	0.00	47.3
dDR02	0.58	40.0	1.26	35.8	dDR-w02	0.65	36.4
dDR03	4.16	9.4	6.34	4.6	dDR-w03	4.24	8.5
					dDR-w04	4.47	7.8
Open-chain D-ribose							
Struc.	ΔE_0	% Pop.	ΔE_0	% Pop.	Struc.	ΔE_0	% Pop.
DR01	0.00	39.4	0.00	47.0	DR-w01	0.00	42.2
DR02	1.48	21.7	4.58	7.4	DR-w02	0.10	40.5
DR03	2.68	13.3	1.05	30.8	DR-w03	2.20	17.3
DR04	3.32	10.3	5.27	5.6			
DR05	3.50	9.6	5.47	5.2			
DR06	4.77	5.7	6.12	4.0			

	PCM M06-2X/6-311++G(d,p)		PCM MP2(full)/ 6-311++(3df,2p)//M06-2X/6-311++G(d,p)//		PCM + explicit H_2O M06-2X/6-311++G(d,p)		
α-2-deoxy-D-ribofuranose							
Struc.	ΔE_0	% Pop.	ΔE_0	% Pop.	Struc.	ΔE_0	% Pop.
dDRαf01	0.00	20.8	0.00	25.8	dDRαf-w01	0.00	39.1
dDRαf02	0.13	19.8	2.70	8.7	dDRαf-w02	0.42	33.0
dDRαf03	0.16	19.5	0.54	20.8	dDRαf-w03	1.54	21.0
dDRαf04	0.56	16.6	0.86	18.2	dDRαf-w04	4.30	6.9
dDRαf05	2.33	8.1	2.69	8.7			
dDRαf06	3.04	6.1	1.98	11.6			
dDRαf07	3.17	5.8	5.07	3.3			
dDRαf08	4.57	3.3	5.40	2.9			
β-2-deoxy-D-ribofuranose							
Struc.	ΔE_0	% Pop.	ΔE_0	% Pop.	Struc.	ΔE_0	% Pop.
dDRβf01	0.00	23.5	0.64	18.7	dDRβf-w01	0.00	46.7
dDRβf02	0.79	17.1	0.00	24.2	dDRβf-w02	1.65	24.0
dDRβf03	1.70	11.8	3.55	5.8	dDRβf-w03	4.36	8.1
dDRβf04	1.80	11.4	2.32	9.5	dDRβf-w04	4.60	7.3
dDRβf05	1.89	11.0	1.81	11.7	dDRβf-w05	4.65	7.1
dDRβf06	3.39	6.0	1.55	13.0	dDRβf-w06	4.76	6.8
dDRβf07	4.19	4.3	3.79	5.3			
dDRβf08	4.23	4.3	4.73	3.6			
dDRβf09	4.44	3.9	6.46	1.8			
dDRβf10	4.65	3.6	3.98	4.9			
dDRβf11	4.99	3.1	6.66	1.5			
α-D-ribofuranose							
Struc.	ΔE_0	% Pop.	ΔE_0	% Pop.	Struc.	ΔE_0	% Pop.
DRαf01	0.00	20.5	0.92	21.9	DRαf-w01	0.00	19.0
DRαf02	0.87	14.5	4.11	6.0	DRαf-w02	0.23	17.3
DRαf03	1.21	12.6	0.00	31.8	DRαf-w03	0.63	14.7
DRαf04	2.07	8.9	3.37	8.2	DRαf-w04	2.27	7.6
DRαf05	2.47	7.6	3.44	7.9	DRαf-w05	2.41	7.2
DRαf06	2.64	7.1	6.70	2.1	DRαf-w06	2.51	6.9
DRαf07	3.04	6.0	5.34	3.7	DRαf-w07	2.74	6.3
DRαf08	3.57	4.9	6.22	2.6	DRαf-w08	3.59	4.5
DRαf09	3.63	4.7	3.91	6.5	DRαf-w09	3.81	4.1
DRαf10	4.22	3.7	5.59	3.3	DRαf-w10	4.06	3.7

DRαf11	4.30	3.6	7.12	1.8	DRαf-w11	4.44	3.2
DRαf12	4.67	3.1	5.68	3.2	DRαf-w12	4.64	2.9
DRαf13	4.98	2.8	8.47	1.0	DRαf-w13	4.98	2.6

β-D-ribofuranose

Struc.	ΔE_0	% Pop.	ΔE_0	% Pop.	Struc.	ΔE_0	% Pop.
DRβf01	0.00	20.7	1.68	9.3	DRβf-w01	0.00	23.1
DRβf02	0.03	20.5	1.00	12.3	DRβf-w02	0.70	17.5
DRβf03	0.69	15.7	0.07	17.9	DRβf-w03	0.72	17.3
DRβf04	2.45	7.7	0.00	18.4	DRβf-w04	1.29	13.8
DRβf05	3.00	6.2	2.80	5.9	DRβf-w05	4.02	4.6
DRβf06	3.40	5.3	0.83	13.2	DRβf-w06	4.11	4.4
DRβf07	3.74	4.6	2.79	6.0	DRβf-w07	4.12	4.4
DRβf08	4.21	3.8	4.48	3.0	DRβf-w08	4.20	4.2
DRβf09	4.42	3.5	3.19	5.1	DRβf-w09	4.53	3.7
DRβf10	4.46	3.4	5.93	1.7	DRβf-w10	4.54	3.7
DRβf11	4.75	3.0	7.38	0.9	DRβf-w11	4.82	3.3
DRβf12	4.96	2.8	4.01	3.6			
DRβf13	4.99	2.8	4.71	2.7			

	PCM M06-2X/6-311++G(d,p)		**PCM MP2(full)/ 6-311++(3df,2p)//M06-2X/6-311++G(d,p)//**		**PCM + explicit H_2O M06-2X/6-311++G(d,p)**	

α-2-deoxy-D-ribopyranose

Struc.	ΔE_0	% Pop.	ΔE_0	% Pop.	Struc.	ΔE_0	% Pop.
dDRαp01	0.00	45.7	0.00	40.5	dDRαp-w01	0.00	40.7
dDRαp02	1.56	24.3	1.28	24.2	dDRαp-w02	0.41	34.5
dDRαp03	1.75	22.6	1.30	24.0	dDRαp-w03	2.37	15.6
dDRαp04	4.50	7.4	3.17	11.3	dDRαp-w04	3.70	9.2

β-2-deoxy-D-ribopyranose

Struc.	ΔE_0	% Pop.	ΔE_0	% Pop.	Struc.	ΔE_0	% Pop.
dDRβp01	0.00	50.5	0.00	56.9	dDRβp-w01	0.00	67.5
dDRβp02	2.66	17.2	4.06	11.1	dDRβp-w02	4.41	11.4
dDRβp03	2.73	16.7	3.61	13.3	dDRβp-w03	4.41	11.4
dDRβp04	2.90	15.6	2.76	18.7	dDRβp-w04	4.79	9.7

α-D-ribopyranose

Struc.	ΔE_0	% Pop.	ΔE_0	% Pop.	Struc.	ΔE_0	% Pop.
DRαp01	0.00	23.0	1.33	22.7	DRαp-w01	0.00	20.5

DRαp02	0.09	22.2	0.00	38.8	DRαp-w02	0.24	18.6
DRαp03	1.41	13.0	4.95	5.3	DRαp-w03	0.65	15.7
DRαp04	1.48	12.7	4.38	6.6	DRαp-w04	1.79	9.9
DRαp05	1.89	10.7	2.37	14.9	DRαp-w05	1.82	9.8
DRαp06	3.03	6.8	4.69	5.8	DRαp-w06	2.18	8.5
DRαp07	3.34	6.0	6.73	2.6	DRαp-w07	2.57	7.3
DRαp08	3.53	5.6	6.09	3.3	DRαp-w08	2.84	6.5
					DRαp-w09	4.61	3.2

β-D-ribopyranose

Struc.	ΔE_0	% Pop.	ΔE_0	% Pop.	Struc.	ΔE_0	% Pop.
DRβp01	0.00	30.9	0.00	45.0	DRβp-w01	0.00	26.6
DRβp02	0.66	23.6	1.94	20.6	DRβp-w02	0.94	18.2
DRβp03	1.00	20.6	1.78	22.0	DRβp-w03	1.69	13.4
DRβp04	1.05	20.2	3.46	11.1	DRβp-w04	2.62	9.2
DRβp05	4.69	4.7	8.73	1.3	DRβp-w05	2.81	8.5
					DRβp-w06	2.99	7.9
					DRβp-w07	3.40	6.7
					DRβp-w08	3.71	5.9
					DRβp-w09	4.95	3.6

[a]$K = -RT \ln\Delta E_0$, where K is the population relationship, R the ideal gas constant, T the absolute temperature and ΔE_0 the relative energy.

In the open-chain 2-deoxy-D-ribose, MP2 single point calculations agree with the energy ranking obtained at M06-2X computational level. However, at B3LYP level, the first M06-2X minimum becomes the fifth most stable conformer with a relative energy of 4.10 kJ mol^{-1} (see Table 2 and a more detailed table in the Supplementary Information). In the open-chain D-ribose, MP2 single point calculations follow the M06-2X order, with the exception of the second and third structures which are inverted at MP2 level. B3LYP results provide the same ranking of the M06-2X calculations only for the first and second minima while the rest of the most stable ones are disordered.

In the case of the furanose configurations, the energy ranking is different for the three methods considered. Only in the α-2-deoxy-D-ribofuranose the most stable minimum is the same at M06-2X and MP2 levels. In the rest of furanose conformers, the most stable minimum at M06-2X corresponds to the second, third and fifth place, for β-2-deoxy-D-ribofuranose, α-D-ribofuranose and β-D-ribofuranose respectively at MP2 level.

In contrast, the pyranose minima show, in general, good consistence between the different methodologies employed. For instance, in α-2-deoxy-D-ribopyranose and β-D-ribopyranose, the energy ranking is the same for the DFT and MP2 calculations, with the exception of the second and third minima of β-D-ribopyranose which are alternated at MP2 level. In β-2-deoxy-D-ribopyranose and α-D-ribopyranose the first minimum coincides for both DFT functionals and the ranking of the most stable minima does not show important differences. However, MP2 calculations for α-D-ribopyranose have less similarity to those obtained at the DFT levels.

Table 3. Boltzmann population[a] in percentage for 2-deoxy-D-ribose and D-ribose at the M06-2X/6-311++G(d,p) and MP2(full)/6-311++G(3df,2p)//M06-2X/6-311++G(d,p) computational levels. Calculations take into account all minima (T = 298.16 K) for every configuration.

	PCM/M06-2X					**MP2[b]**					**(PCM + H_2O)/M06-2X[c]**				
Structure	Open	α-fur	β-fur	α-pyr	β-pyr	Open	α-fur	β-fur	α-pyr	β-pyr	Open	α-fur	β-fur	α-pyr	β-pyr
2-deoxy-D-ribose	0.0	0.6	0.3	86.6	12.5	0.0	0.6	0.1	91.3	8.0	0.0	1.4	0.4	73.4	24.8
D-ribose	0.0	0.1	0.1	71.0	28.8	0.0	0.1	0.0	71.6	28.3	0.0	0.1	0.1	69.2	30.6

[a]$K = -RT \ln\Delta E_0$, where K is the population relationship, R the ideal gas constant, T the absolute temperature and ΔE_0 the relative energy.

[b]In the case of MP2(full) calculations, only for the most stable minima, *i.e.*, with relative M06-2X energies less than 5 kJ mol^{-1}.

[c](PCM + H_2O)/M06-2X calculations: an explicit molecule of water was added to the most stable implicit minima, *i.e.*, less than 3 kJ mol^{-1}.

The population of the different configurations for the 2-deoxy-D-ribose and D-ribose using all the minima obtained at the DFT levels are gathered in Table 3. Analogous population results are obtained at M06-2X and MP2 levels. In the two molecules studied, the α-pyranose conformers are the most populated, followed by the β-pyranose ones. Only B3LYP results indicate the presence of significant populations of open-chain and furanose forms. Besides, Barnett *et al.*[58] analyzed the furanose (β-D-ribofuranose) and pyranose (β-D-glucopyranose) free energy pucker surfaces and volumes in water solutions using AM1, PM3, PM3CARB-1 and SCC-DFTB semiempirical potentials. A comparison with DFT optimized structures and at Hartree-Fock (HF) free energy surface revealed that SCC-DFTB provided the best semiempirical description of five- and six-membered carbohydrate ring deformation. Also, Dowd *et al.*[59] carried out a MM3 modeling of D-ribose and 2-deoxy-D-ribose ring

puckering with an implicit solvation model in order to simulate the solvent effects. They concluded from experimental and theoretical results that several tautomeric forms of the two monosaccharides exist in multiple conformations in solution. The authors pointed out that the discrepancies between their calculated energies and the free energies derived from NMR results were less than 1.0 kcal mol^{-1}, concluding that the equilibrium between conformers was not very accurately predicted. Finally, it seems that the M06-2X functional is a good choice for the system under study. Although, the M06-2X functional is more computationally demanding than the B3LYP functional, while less than MP2, it performs well as it predicts structures, energies, and harmonic spectra quite accurately.[60]

2. AIM and NBO analysis of the intramolecular weak interactions.

Atoms in Molecules (AIM)[43,44] and Natural Bond Orbital (NBO)[51] methodologies provide a set of interesting tools for the analysis of the intramolecular weak interactions. The main group of weak interactions which take place in the 2-deoxy-D-ribose and D-ribose carbohydrates studied in the present work is the hydrogen bonds (HB).

The topological approach of AIM establishes that an HB is characterized by the presence of a bond critical point (BCP) which, through a bond path, links to nuclear attractors: one hydrogen atomic center and on electronegative (oxygen) atomic center. The electron density and its Laplacian at BCP present positive but small values compared, in absolute terms, to those computed for covalent bonds. The orbital approach of NBO indicates that a HB is associated to the charge transfer between a lone pair (LP) on the acceptor moiety and the σ* (antibonding) orbital of the donor moiety which includes the hydrogen atom.

The types of HB formed between two hydroxyl groups and even between one hydroxyl group and the aldehyde moiety in the case of the open-chain forms, can be grouped using the profile of the electron density, ρ, its Laplacian, $\nabla^2\rho$, and the second-order perturbation NBO energy, $E^{(2)}$, versus the geometrical distance attending to the number of skeleton carbon atoms which separate the interacting functional groups (**Scheme 1**).[1] Thus, the interactions present in these compounds can be classified *a priori* as: 1-2, 1-3, 1-4 and 1-5 type interactions.

Scheme 1. HB interactions in 2-deoxy-D-ribose and D-ribose: (*a*) 1-2, (*b*) 1-3, (*c*) 1-4 and (*d*) 1-5.

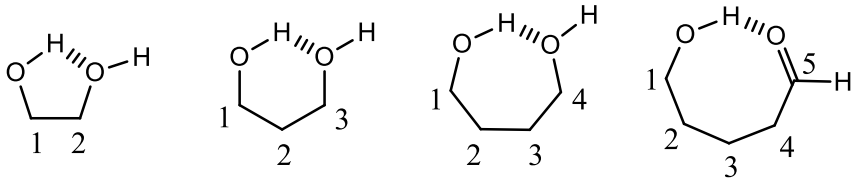

(*a*) (*b*) (*c*) (*d*)

As can be seen in Figure 5, for all minima in 2-deoxy-D-ribose and D-ribose with total relative energy less than 10 kJ mol^{-1}, the electron density at BCP (*a*), its Laplacian (*b*), and $E^{(2)}$ NBO energy (*c*), exhibit exponential relationships versus the O···H interatomic distance, in agreement with previous reports.[61-63] In all of them, the type of interaction can be classified, specially using $\nabla^2\rho_{O\cdots H}$, in three main groups the 1-2 (pseudo-five membered ring), 1-3 (pseudo-six membered ring) and 1-4 plus 1-5 (pseudo-seven and pseudo-eight membered rings). Additionally, a relationship is observed between $E^{(2)}$ NBO energy *versus* the electron density (ρ), establishing a correlation between a topological and an orbital variables.

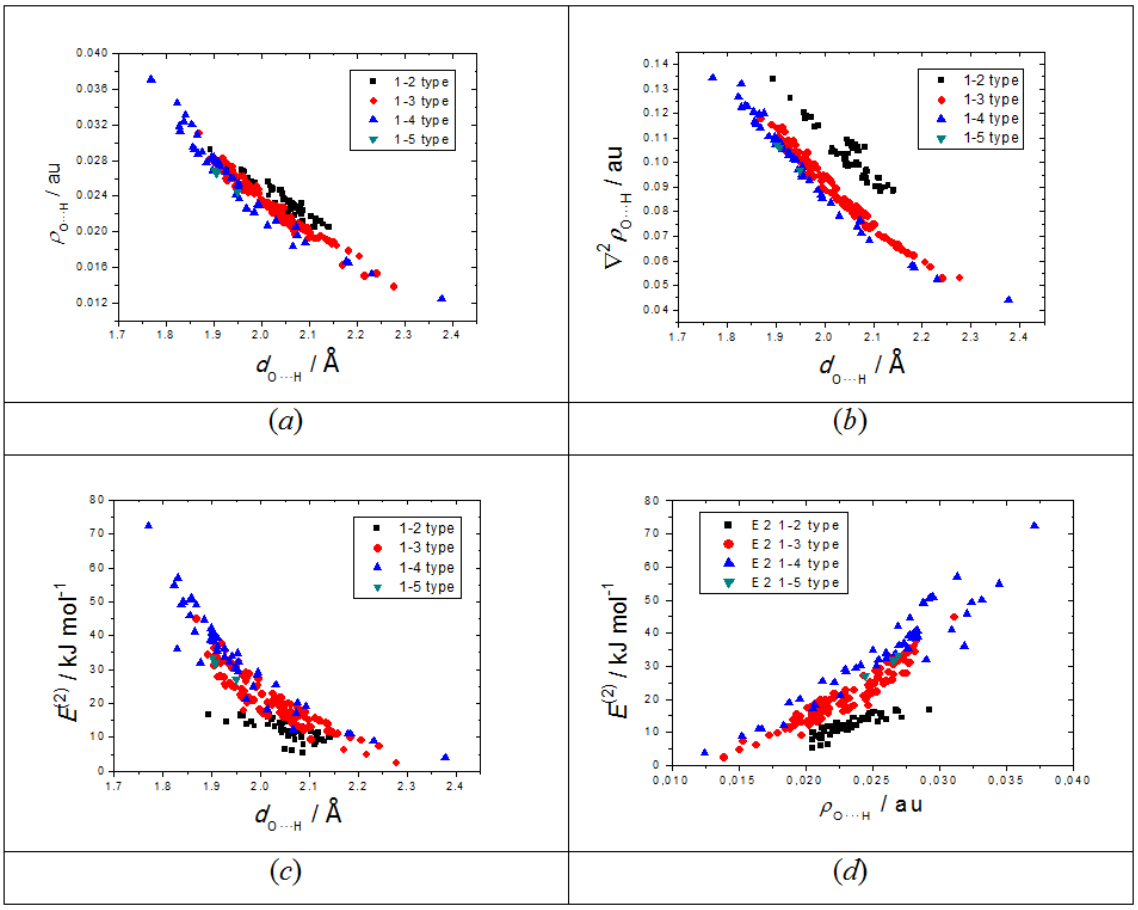

Figure 5. Representation of (*a*) electron density $\rho_{O\cdots H}$ at the BCP in au; (*b*) its Laplacian $\nabla^2\rho_{O\cdots H}$ in au; and (*c*) $E^{(2)}$ NBO energy in kJ mol^{-1} *versus* the O···H interatomic distance in Å. In (*d*) is represented the $E^{(2)}$ NBO energy *versus* the electron density. Black squares refer to 1-2 type interactions, red circles to 1-3 ones, blue triangles to 1-4 ones and green inverse triangles to 1-5 ones. All data extracted from all minima in 2-deoxy-D-ribose and D-ribose with relative energy less than 10 kJ mol^{-1}.

1-2 type interactions present a smaller range of values than 1-3 or 1-4 ones in the geometrical and even in the topological and orbital parameters. 1-2 type interactions range between 1.89 and 2.14 Å, 113 and 121 deg, 0.020 and 0.029 au for the electron density and 0.088 and 0.134 au for its Laplacian, and finally, 5.23 and 16.78 kJ mol^{-1} for $E^{(2)}$. Furthermore, 1-3 type interactions are between 1.87 and 2.28 Å, 123 and 144 deg, 0.014 and 0.031 au for the electron density and 0.053 and 0.118 au for its Laplacian, and finally, 2.51 and 45.02 kJ mol^{-1} for $E^{(2)}$. In 1-4 type interactions the intervals increase with respect to this last one, being the upper limit in $E^{(2)}$, 72.34 kJ mol^{-1}.

Good exponential correlations between the two topological variables, ρ and $\nabla^2\rho$, *versus* the interatomic distance are found for 1-3 and 1-4 type interactions, with R^2 larger than 0.97. In contrast, for 1-2 type interactions the R^2 values are only 0.89 and 0.83 for the ρ and $\nabla^2\rho$, respectively. Two sets of points are observed for this kind of 1-2 interactions when the Laplacian is represented (Figure 5, panel *b*). One group of points is concentrated in a very small interval of distances (between 2.05 and 2.10 Å), and shows an unclear pattern with regard to the interacting atoms, which deviates from the expected behavior. The representation of the geometrical O···H–O angle *versus* the interatomic O···H distance, shows hat these points belong to 1-2 type interactions between the aldehyde moiety and the hydroxyl group (attached to C2) of the open-chain D-ribose with geometrical angles less than 117º.

The explicit water molecule plays a key role in the stabilization of sugars' conformation. In the most stable minima it forms an intermolecular bridge, acting both as HBA and HBD. The electron density at the BCP of the intermolecular sugar-H_2O HBs ranges between 0.005 and 0.040 au, and its Laplacian, between 0.019 and 0.141 au, being its upper limit larger than in the intramolecular ones. The NBO $E^{(2)}$ energies are in an interval between 2.41 and 59.89 kJ mol^{-1}.

3. Non-chiroptical vibrational study: IR and Raman spectroscopies.

Figures 6 and 7 show the IR and Raman spectra of D-ribose and 2-deoxy-D-ribose, recorded in H_2O and D_2O solutions and in the solid phase (powder sample), compared with the theoretical spectra of the most stable set of α-pyranose and β-pyranose anomers, which are the most populated according to the quantum chemical calculations in PCM-water (M06-2X/6-311++G(d,p) and B3LYP/6-311++G(d,p)) and PCM plus an explicit water molecule (M06-2X/6-311++G(d,p)), and expected to be mainly present in aqueous solutions. Figures S5 to S12 of the Supplementary Information material provide an extensive comparison of the experimental and theoretical results for those readers interested in a more detailed analysis.

The theoretical spectra have been weighted according to the predicted populations of the most stable conformers (see Table 3). As shown in Figures 6 and 7 (panels *b* and *d*) and discussed below, the experimental spectra seem to prove the presence of open-chain structures in the case of 2-deoxy-D-ribose in solution. Thus, in spite of the fact that the PCM and PCM + H_2O M06-2X calculations do not predict the presence of those

forms, the predicted B3LYP populations for open-chain forms, that is, around 2.3% for D-ribose and 8.9% for 2-deoxy-D-ribose, were assumed in all the theoretical spectra shown in the Figures 6, 7, 8 and 9**.**

In general, our theoretical spectra for both carbohydrates are in good agreement with the experimental ones. The PCM theoretical spectra agree well with experimental spectra, but there are some regions in which the theoretical results are improved when an explicit molecule of water is added to continuum solvent calculations. Firstly, focusing our attention in the IR spectra of D-ribose, we can see that the 1600-1400 cm^{-1} region, where C–O–H and H_2O bendings are present, and the 700-500 cm^{-1} one are in better agreement with the use of the PCM + H_2O M06-2X calculation. For 2-deoxy-D-ribose something similar occurs. The 1600-1400 cm^{-1} region is better predicted again and, in this case, also the 900-800 cm^{-1} one, which involves ring deformations. Secondly, the Raman spectra of these carbohydrates also show a region where the PCM + H_2O model works better than the PCM alone one. For instance, the 1450-1200 cm^{-1} region, with contributions of C–O–H bend., C–H wagg. and CH_2 rocking. Besides, our Raman spectrum for D-ribose in aqueous solution agrees well with that obtained by Wen *et al.* in the 1600-600 cm^{-1}.[24]

Our main spectral features can confirm the major presence of pyranoses and even if the furanose forms were present in the aqueous solutions, most of the bands which could be assigned to furanose forms, can also be assigned to the pyranose structures. In fact, many bands which appear in the theoretical spectra of the furanoses appear at the same wavenumbers in those of pyranoses. Thus, we cannot confirm the presence of furanoses, adding the fact that, theoretically, pyranoses are much more stable than furanose forms. Moreover, some theoretical intense bands proper of furanoses do not appear in the experimental spectra. Thus, in Raman spectrum of 2-deoxy-D-ribose, our bands at 1263 cm^{-1}, 556 cm^{-1} and at 512 cm^{-1} are well predicted with the contribution of pyranose forms, but these bands are predicted to be very weak for the furanose forms. Mathlouthi *et al.*[16] assigned the presence of furanose forms to Raman bands which appeared at 1186 cm^{-1} (very weak), 1082 cm^{-1} (strong) and at 512 cm^{-1} (medium). However, our theoretical spectra of pyranose forms reproduce well these bands and furanose forms ones reproduce them weaker. If we assign these bands to furanose forms, we would have to observe two bands of comparable intensity at 813 cm^{-1} and at 874 cm^{-1}. Also, pyranoses reproduce them with different intensity, as we can also see experimentally. Moreover, the 1400-1200 cm^{-1} region is better reproduced by pyranose

forms than by furanose forms. Besides, in IR spectra of this monosaccharide, the bands observed at 1010 cm^{-1} and at 977 cm^{-1} are better predicted by the pyranose model.

If we focus our attention on the Raman spectra of D-ribose, we can see that the intense bands at 1469 cm^{-1}, 1260 cm^{-1}, 1121 cm^{-1} and at 1078 cm^{-1} are better structured by theoretical spectra of pyranoses, and they are predicted less intense by furanose ones. Mathlouthi *et al.*[16] assigned the Raman bands at 1158 cm^{-1} (shoulder), 1078 cm^{-1} (strong), 916 cm^{-1} (weak), 830 cm^{-1} (very weak), 596 cm^{-1} (weak) and at 462 cm^{-1} (weak) to the presence of furanose forms. If we assign these bands to the presence of furanose forms, we would also observe a band at 1185 cm^{-1} in the experimental spectra and we do not see this feature. On the contrary, IR features of furanose and pyranose forms are more similar for this carbohydrate and it is difficult to get a clear conclusion with the only assignment of the IR patterns.

Only taking into account the most stable set of pyranose conformers (up to 5 kJ mol^{-1}), the experimental spectra can be reproduced in a suitable way, especially whole Raman spectra and 1200-900 cm^{-1} region in IR ones. The populations of the open-chain forms are predicted to be about 2.3% for D-ribose and 8.9% for 2-deoxy-D-ribose (B3LYP), which contribute to the total theoretical vibrational spectra of these species with an additional band at 1650 cm^{-1}, corresponding to the normal mode associated to C=O stretching (or C=C stretching for the enediol form), which is observed experimentally as a weak band in Raman and IR spectra of their aqueous solutions. But nothing can be confirmed in the IR case because water absorbs at this wavenumber. So, the IR and Raman spectra in D_2O solutions were recorded in order to throw light on this point. However, the band was not observed in the spectra of D-ribose. On the contrary, and according to the quantum chemical calculations which predict a higher population of open-chain forms for 2-deoxy-D-ribose, the band appears in IR spectra of D_2O solution of this last monosaccharide. The fact that this band appears in Raman spectrum of the aqueous solution in the case of D-ribose and not in D_2O, and that it is observed stronger in H_2O solution than in D_2O for 2-deoxy-D-ribose is logical. The explanation is that the D–O···D bond is less favored than H–O···H one, consequently the formation of open-chain forms is a reaction less assisted in D_2O solution, considering also that an hydrogen is necessary to start it.[64,65] Nevertheless, in the solid Raman and IR spectra this band is not observed, and they are in fair agreement with theoretical ones only considering pyranose forms. Consequently, we can conclude that α-pyranose and β-

pyranose forms are present in the solid state, being majority, as it was reported by Šišak *et al.*[18]

Besides, Raman spectra in aqueous solution changing the temperature were recorded for the two carbohydrates (see Figure 8). There were no appreciable changes in spectral features. In fact, the band at 1650 cm^{-1} did not increase as a function of temperature.[17] Perhaps an addition of acid catalyst could assist the creation of open-chain forms.[66]

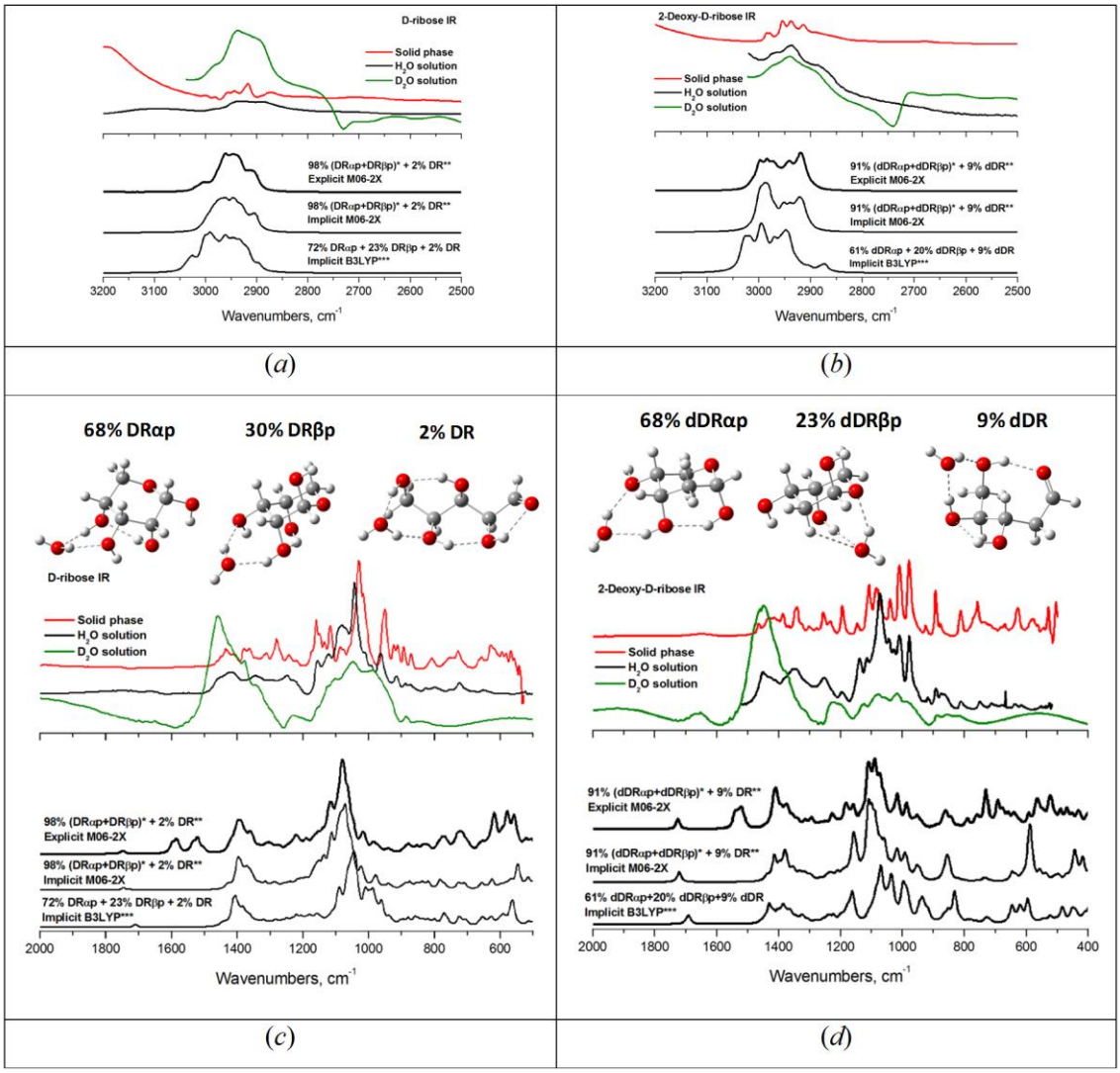

*PCM/M06-2X populations of pyranose forms of D-ribose and 2-deoxy-D-ribose are 71% DRαp:29% DRβp and 87% dDRαp:13% dDRβp. (PCM + H_2O)/M06-2X populations of pyranose forms of D-ribose and 2-deoxy-D-ribose are: 69% DRαp:31% DRβp and 75% dDRαp:25% dDRβp. These populations are multiplied by 0.98 and 0.91, respectively, in order to get 100% when open-chain forms are added.

**Populations of open-chain forms coming from the B3LYP calculations.

***B3LYP populations do not sum 100% because of the percentages of 10% and 3% of furanose forms for 2-deoxy-D-ribose and for D-ribose, respectively.

Figure 6. Experimental (top) and scaled predicted (bottom) IR spectra of D-ribose (panels *a* and *c*) and 2-deoxy-D-ribose (panels *b* and *d*) in the 3200-2500 cm^{-1} and 2000-400 cm^{-1} spectral regions. In the four panels, experimental IR spectra in solid phase (in red), H_2O (in black) and D_2O (in green) solutions are shown at the top. The solutions of H_2O and D_2O were prepared with a molarity of 4. At the bottom, theoretical spectra are weighted with the population of the most stable conformers. NIST scaling frequency factor of 0.967 (B3LYP) and 0.95 (M06-2X), Lorentzian function, pitch = 1 cm^{-1}, FWHM (Full Width Half Maximum) = 8 cm^{-1}.

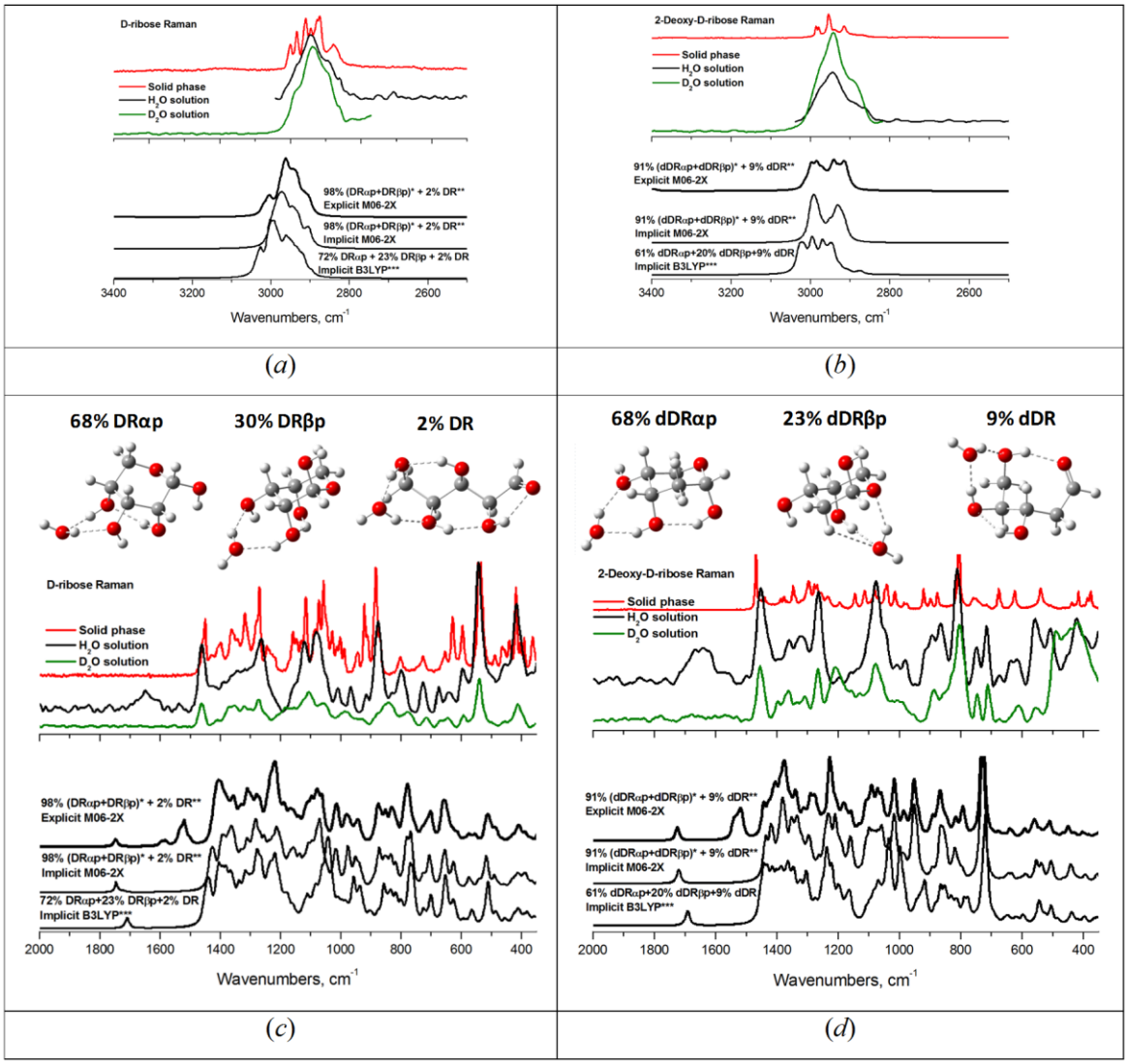

*PCM/M06-2X populations of pyranose forms of D-ribose and 2-deoxy-D-ribose are 71% DRαp:29% DRβp and 87% dDRαp:13% dDRβp. (PCM + H_2O)/M06-2X populations of pyranose forms of D-ribose and 2-deoxy-D-ribose are: 69% DRαp:31% DRβp and 75% dDRαp:25% dDRβp. These populations are multiplied by 0.98 and 0.91, respectively, in order to get 100% when open-chain forms are added.

**Populations of open-chain forms coming from the B3LYP calculations.

***B3LYP populations do not sum 100% because of the percentages of 10% and 3% of furanose forms for 2-deoxy-D-ribose and for D-ribose, respectively.

Figure 7. Experimental (top) and scaled predicted (bottom) Raman spectra of D-ribose (panels *a* and *c*) and 2-deoxy-D-ribose (panels *b* and *d*) in the 3400-2500 cm^{-1} and 2000-350 cm^{-1} spectral regions. In the four panels, experimental Raman spectra in solid phase (in red), H_2O (in black) and D_2O (in green) solutions are shown at the top. The solutions of H_2O and D_2O were prepared with a molarity of 4. At the bottom, theoretical spectra are weighted with the population of the most stable conformers. NIST scaling frequency factor of 0.967 (B3LYP) and 0.95 (M06-2X), Lorentzian function, pitch = 1 cm^{-1}, FWHM (Full Width Half Maximum) = 8 cm^{-1}.

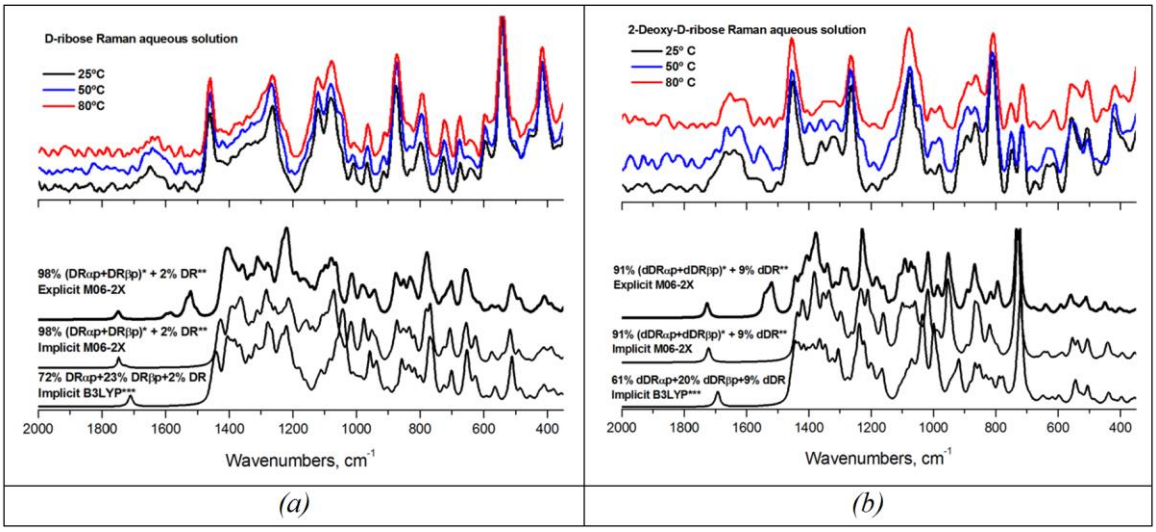

*PCM/M06-2X populations of pyranose forms of D-ribose and 2-deoxy-D-ribose are 71% DRαp:29% DRβp and 87% dDRαp:13% dDRβp. (PCM + H_2O)/M06-2X populations of pyranose forms of D-ribose and 2-deoxy-D-ribose are: 69% DRαp:31% DRβp and 75% dDRαp:25% dDRβp. These populations are multiplied by 0.98 and 0.91, respectively, in order to get 100% when open-chain forms are added.

**Populations of open-chain forms coming from the B3LYP calculations.

***B3LYP populations do not sum 100% because of the percentages of 10% and 3% of furanose forms for 2-deoxy-D-ribose and for D-ribose, respectively.

Figure 8. Experimental (top) and scaled predicted (bottom) Raman spectra of D-ribose (*a*) and 2-deoxy-D-ribose (*b*) in the 2000 cm^{-1}-350 cm^{-1} spectral region. In the two panels, experimental Raman spectra in aqueous solution with changes of temperature: 25 ºC (in black), 50 ºC (in blue) and 80 ºC (in red) at the top. The solutions were prepared with a molarity of 4. At the bottom, theoretical spectra are weighted with the population of the most stable conformers of α-pyranose, β-pyranose and open-chain forms according to the PCM/B3LYP and the PCM and PCM +H_2O M06-2X methods,

being assumed B3LYP population for open-chain forms. NIST scaling frequency factor of 0.967 (B3LYP) and 0.95 (M06-2X), Lorentzian function, pitch = 1 cm^{-1}, FWHM (Full Width Half Maximum) = 8 cm^{-1}.

4. Chiroptical vibrational response: VCD spectroscopy.

Because of the chirality of D-ribose and 2-deoxy-D-ribose, it was expected that some interesting structural information of both monosaccharides could be obtained from a detailed study of their Vibrational Circular Dichroism (VCD) spectra. For this reason, we recorded the VCD spectra of solid (mulls and thin films) and solution (H_2O and D_2O) samples of both carbohydrates, and then, they were analyzed by comparison with those calculated from the (PCM + H_2O)/M06-2X and the PCM M062X-B3LYP methods. If we compare our results with those obtained by Tummalapalli *et al.*[20] we can find two couplets which appear in both works, *i.e.*, one (–,+) couplet with components at 1265 cm^{-1} and at 1240 cm^{-1} of D-ribose-$(OD)_4$ and the (–,+) other one at 1159 cm^{-1} and at 1125 cm^{-1} in D-ribose-$(OH)_4$, both in DMSO-d_6 solution. Tummalapalli *et al.* do not reproduce neither the first one in the D-ribose-$(OH)_4$ spectrum nor the second one in the D-ribose-$(OD)_4$ one. On the contrary, we observe the two couplets in all our spectra. They do not include the exocyclic C–O stretching motions of the D-ribose for their correlation about the structural details and VCD of deuterated D-sugars, because of the different signs of the two bands at 1159 cm^{-1} and at 1125 cm^{-1}. They concluded that the VCD feature at 1150 cm^{-1} indicates that the overall orientation of hydroxyl groups can be deduced from the VCD studies. Concerning the C–O–H and C–C–H bending motions, they do not obtain measurable VCD features for D-ribose (detailed explanation is provided in the ref. 20).

Later, Bose et *al.*[21] complemented these last results for D-ribose with the analysis of the VCD spectrum of this carbohydrate in DMSO-d_6 solution with the use of improved VCD instrumentation. The VCD pattern that these authors observed in their spectrum and that we also observed in our spectra of D-ribose in H_2O and D_2O solutions is the (+,–,+) structure at 1347 cm^{-1}, at 1263 cm^{-1} and at 1225 cm^{-1} (broad band). They also observed a (–,+) couplet with components at 1460 cm^{-1} and at 1435 cm^{-1}, which was weaker in our spectra. But the (–,–,–) bands observed by authors of ref. 21 at 1337 cm^{-1}, at 1311 cm^{-1} and at 1287 cm^{-1} appeared in our spectra with different sign (+,+,+). It could be due to the signal/noise ratio, because we measured the spectra in solution with

14000-28000 scans by blocks of 2000 scans, that is around 10 hours, and Bose et *al.* used 1 hour of measurement for those spectra.

At this point we can focus the discussion on our results. In the same way that for the analysis of the IR and Raman spectra, the PCM + H_2O model improves some VCD features of both carbohydrates. Thus, for the VCD spectrum of D-ribose in water solution, the (+,+,–,–) bands at 1125, 1089, 1056 and 1037 cm^{-1} are better predicted. In the case of 2-deoxy-D-ribose, it occurs for the (–,+) couplet at 1116 and 1077 cm^{-1}. The analysis of the VCD bands, intensity and signs, observed and calculated for D-ribose and 2-deoxy-D-ribose, has been very helpful to conclude the presence of their α- and β-pyranose forms both in the solid and solution phases. The next paragraphs stand out the main VCD results obtained in this work in the CH stretching and 2000-900 cm^{-1} spectral regions.

In relation to CH stretching region, the two VCD spectra in D_2O solution (see Figure 9 panels *a* and *b*) display a sequence of positive CH stretching bands, which is consistent with the signs observed in the spectra of the B3LYP and M06-2X calculations. Thus: i) for D-ribose, the (+,+,+) pattern at 3016, 2993 and 2970 cm^{-1} can be observed in D_2O solution and is well predicted by theoretical spectra. ii) Concerning 2-deoxy-D-ribose, we can remark about the agreement of some relevant bands again. In D_2O solution, the (+,+,+,+) bands at 2988, 2969, 2946 and 2927 cm^{-1} are well predicted by the theoretical spectra.

Figure 9 (panels *c* and *d*) shows VCD spectra of D-ribose and 2-deoxy-D-ribose in different conditions, *i.e.*, H_2O and D_2O solutions and in the solid phase (thin film and fluorolube/nujol mulls) in the 2000-900 cm^{-1} spectral region, compared with the theoretical spectra previously stated. As in the preceding cases, they are in good agreement. The presence of pyranose forms is enough in order to reproduce the experimental VCD spectra. We can support this fact by the sign and position of several VCD features in the C–H wagging, C–O–H bending and C–O stretching regions, that is, for instance: i) for D-ribose, the (–,+) couplet at 1441 and 1421 cm^{-1} can be observed in the fluorolube mull spectrum and is well predicted by theoretical spectra. In addition, in film and solutions spectra another interesting (+,–) couplet is observed at 1170 and 1154 cm^{-1} and a sequence of (+,+,–,–) bands at 1125, 1089, 1056 and 1037 cm^{-1} are both also in good agreement with theoretical data. ii) Concerning 2-deoxy-D-ribose, we can remark, likewise, the agreement of some relevant bands again. Thus, in its fluorolube mull spectrum, the (+,+,+,–,+) bands sequence at 1378, 1365, 1346, 1340 and 1313 cm^{-}

[1] and, in its film and solutions spectra, the (–,+,–,+,–) bands set at 1191, 1153, 1116, 1077 and 977 cm^{-1} match well newly the experimental and theoretical results.

All the observed VCD features in both solutions (H_2O and D_2O) and solid phase (thin films and mulls) are in good agreement, *i.e.*, the main VCD features (intensity and signs) are conserved and only small frequency shifts are observed because of the different phases.

In summary, through the analysis of the chiroptical properties of D-ribose and 2-deoxy-D-ribose in relation with their structures, we can confirm the major presence of α- and β-pyranose forms both in solution and solid phases, being the first ones in major proportion in both monosaccharides with a α/β ratio of 3:1, approximately in the two phases. In addition, IR and Raman spectroscopies seem to indicate the existence of a small amount of open-chain forms in the case of 2-deoxy-D-ribose in D_2O and H_2O solutions. Furanose forms could be present but it was not possible to observe any spectral feature which could be unambiguously assigned to the presence of furanose structures. For further comparison see Supplementary Information. Our conclusions in terms of pyranose forms are in good agreement with those obtained in the literature.[15-18,20,21,24,67] On the contrary, those references conclude the presence of a non negligible amount of furanose forms, in different percentages, and our results are not able to reproduce this finding because all the spectral patterns which could be associated to furanose forms are also well reproduced with the presence of pyranose ones.

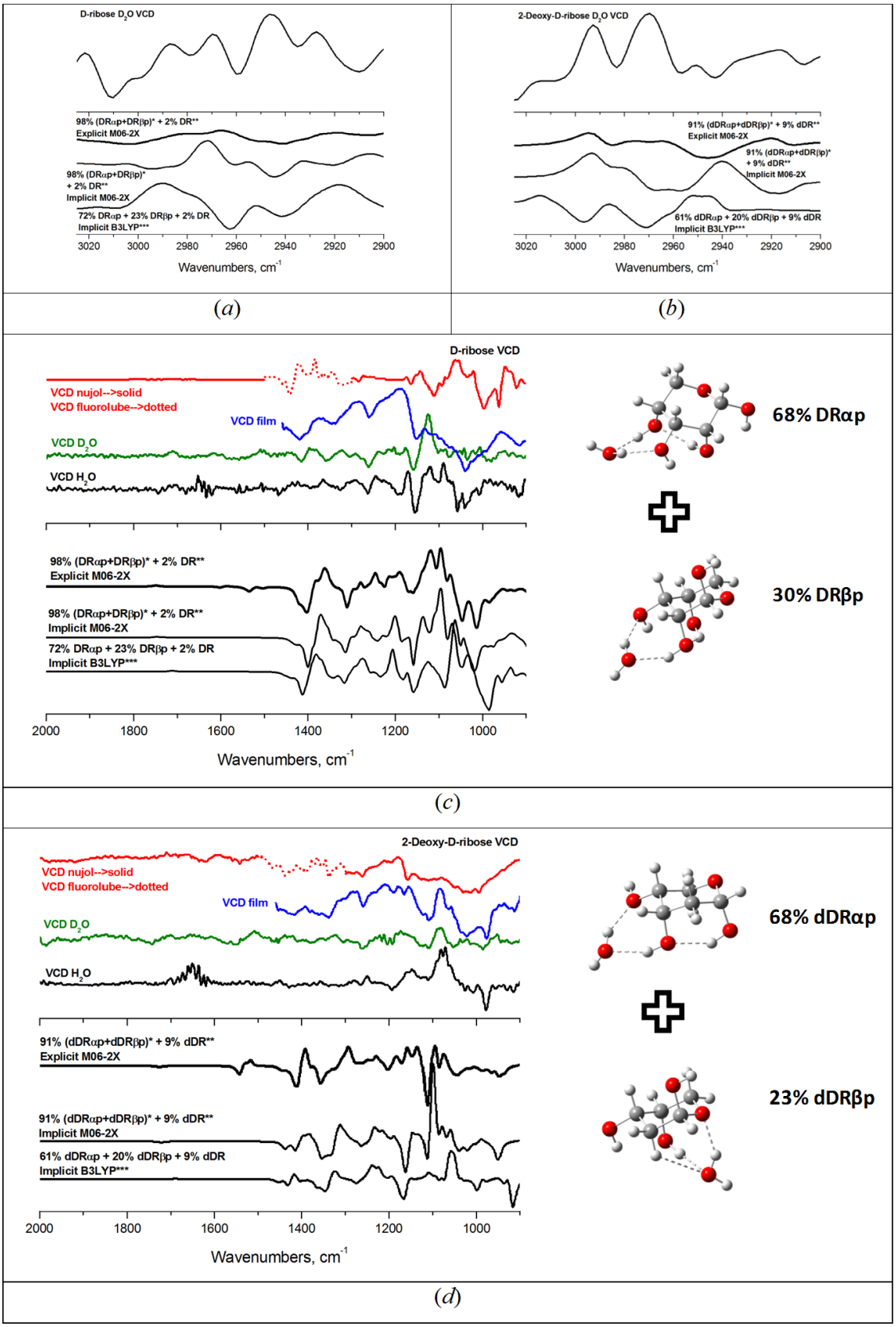

*PCM/M06-2X populations of pyranose forms of D-ribose and 2-deoxy-D-ribose are 71% DRαp:29% DRβp and 87% dDRαp:13% dDRβp. (PCM + H_2O)/M06-2X populations of pyranose forms of D-ribose and 2-deoxy-D-ribose are: 69% DRαp:31% DRβp and 75% dDRαp:25% dDRβp. These populations are multiplied by 0.98 and 0.91, respectively, in order to get 100% when open-chain forms are added.

**Populations of open-chain forms coming from the B3LYP calculations.

***B3LYP populations do not sum 100% because of the percentages of 10% and 3% of furanose forms for 2-deoxy-D-ribose and for D-ribose, respectively.

Figure 9. Experimental (top) and scaled predicted (bottom) VCD spectra of D-ribose (panels *a* and *c*) and 2-deoxy-D-ribose (panels *b* and *d*) in the 3025-2900 cm^{-1} and 2000-900 cm^{-1} spectral regions. Top) Experimental VCD spectra in D_2O solutions (*a* and *b*) and experimental VCD spectra in fluorolube (dotted line in red) and nujol mulls (solid line in red), film (in blue), D_2O (in green) and H_2O (in black) solutions (*c* and *d*). The solutions of H_2O and D_2O were prepared with a molarity of 4. Bottom) Theoretical spectra are weighted with the population of the most stable conformers of α-pyranose, β-pyranose and open-chain forms according to the PCM/B3LYP and the PCM and PCM + H_2O M06-2X methods, being assumed B3LYP population for open-chain forms. NIST scaling frequency factor of 0.967 (B3LYP) and 0.95 (M06-2X), Lorentzian function, pitch = 1 cm^{-1}, FWHM (Full Width Half Maximum) = 8 cm^{-1}.

CONCLUSIONS

1) The most stable set of conformers of each form was determined thanks to an exhaustive analysis of the quantum chemical energies. Five possible configurations for both carbohydrates were studied: open-chain, α-pyranose, β-pyranose, α-furanose and β-furanose forms. A large number of conformational minima were obtained, especially for the open-chain configurations. The pyranose and furanose conformations have been characterized using the Cremer–Pople puckering parameters (P, θ, ϕ). In the two molecules studied, the α-pyranose conformers are the most populated, followed by the β-pyranose ones. Only B3LYP results indicate the presence of significant populations of open-chain and furanose forms, in contrast with the results obtained using the M06-2X hybrid functional.
2) According to our results for these types of molecules, the M06-2X functional is recommended, instead of the B3LYP one, in order to obtain better results with regard to the estimation of their relative populations and the interpretation of their IR, VCD and Raman spectra. Thus, some conclusions can be reached: (i) MP2 and M06-2X approaches give similar results in terms of relative energy; (ii) even in those cases that the B3LYP functional provides similar structures to the MP2 and M06-2X

levels, the calculated relative energies are, in general, very different; (iii) the experimental data agree better with the M06-2X and MP2 results than with B3LYP ones; (iv) the predicted B3LYP populations for the open-chain forms reproduce better the experimental data than those performed at the M06-2X and MP2 methods.

3) Intramolecular hydrogen bonds (HB) are the most important weak interactions taking place in 2-deoxy-D-ribose and D-ribose. Four kinds of them are found attending to the number of atoms of the carbon skeleton, which separate the interacting groups: 1-2, 1-3, 1-4 and 1-5. Geometrical, topological and orbital parameters show narrower ranges of values in 1-2 type than in the rest of the cases. Correlation has been obtained when the electron density, its Laplacian and the $E^{(2)}$ NBO energy are represented versus the interatomic distance. Also, a correlation was observed between $E^{(2)}$ and the electron density.
4) The experimental and theoretical spectra agree well for both carbohydrates. The implicit model reproduces well the experimental spectra, but there are some spectral regions in which the theoretical results are improved when an explicit molecule of water is added to continuum solvent calculations.
5) The IR and Raman spectra in solution and in solid phase show evidence of the major presence of α- and β-pyranose forms, being the first ones in major proportion as much for D-ribose as for 2-deoxy-D-ribose, with an α/β ratio of 3:1, approximately. Besides, these spectroscopies throw light on the presence of open-chain forms in solution in the case of 2-deoxy-D-ribose, because of the presence of a weak band at 1650 cm^{-1}.
6) Through the analysis of the chiroptical properties of D-ribose and 2-deoxy-D-ribose, in relation with their structures, by means of Vibrational Circular Dichroism (VCD), the major presence of pyranose forms was confirmed not only in solution but also in solid phase. However, the existence of open-chain forms was not rechecked because of too weak VCD signals.
7) Furanose forms could be present but it was not possible to observe any spectral feature which could be unambiguously assigned to the presence of furanose structures. In fact, all the spectral patterns which could be associated to furanose forms are also well reproduced with the presence of pyranose ones.
8) The results obtained in this work could be useful for the study of building blocks which contain D-ribose or 2-deoxy-D-ribose. In addition, we have proved the utility of the methodology here employed in order to explore the conformational landscapes

of the two monosaccharides studied. In this way, we think it could likewise be applied to analyze other carbohydrates in biological-like conditions.

ASSOCIATED CONTENT

Supporting Information.

Supplementary data associated with this article can be found in the online version at http://pubs.acs.org. SI1) Detailed tables of energies (kJ mol^{-1}) and populations; SI2) The most stable conformers of the furanose (α- and β-) forms of 2-deoxy-D-ribose and D-ribose in PCM and PCM plus an explicit water molecule calculated at the M06-2X/6-311++G(d,p) computational level; SI3) The most stable conformers of the five forms of 2-deoxy-D-ribose and D-ribose in PCM-water calculated at the M06-2X/6-311++G(d,p) computational level; and SI4) Comparisons between IR, Raman and VCD experimental spectra and PCM theoretical spectra, showing the theoretical contribution of each form for the most stable conformers (α-pyranose, β-pyranose, α-furanose, β-furanose and open-chain) of the two monosaccharides.

AUTHOR INFORMATION

Corresponding authors.

*Authors to whom correspondence should be addressed.
IA) email: ibon@iqm.csic.es; URL: http://are.iqm.csic.es/
JJL) email: jjlopez@ujaen.es; URL: http://vicinv.ujaen.es/octh?ponencia=4&grupo=34

NOTES

The authors declare no competing financial interest.

ACKNOWLEDGMENTS

MMQM thanks the University of Jaén by a predoctoral fellowship. LMA thanks MICINN for a PhD grant (No. BES-2010-031225). This work has been supported by

the Junta de Andalucía (project P08-FQM-04096), MINECO (Project No. CTQ2012-35513-C02-02) and the Comunidad Autónoma de Madrid (Project MADRISOLAR2, ref. S2009/PPQ-1533). Gratitude is also due to University of Jaén for continuing financial support and its CICT for instrumental facilities and to the CESGA and CTI (C.S.I.C.) for an allocation of computer time.

REFERENCES

(1) Azofra, L. M.; Alkorta, I.; Elguero, J.; Popelier, P. L. A. Conformational study of the open-chain and furanose structures of D-erythrose and D-threose. *Carbohydr. Res.* **2012**, *358*, 96-105.

(2) Aviles-Moreno, J.-R.; Huet, T. R. Sugars in the gas phase: The conformational properties of erythrose, threose, and erythrulose characterized by quantum chemistry calculations. *J. Mol. Struc.: THEOCHEM* **2008**, *858*, 113-119.

(3) Cocinero, E. J.; Lesarri, A.; Écija, P.; Basterretxea, F. J.; Grabow, J.-U.; Fernández, J. A.; Castaño, F. Ribose Found in the Gas Phase. *Angew. Chem. Int. Ed.* **2012**, *124*, 3173-3178.

(4) Stern, J. H.; Hubler, P. M. Hydrogen bonding in aqueous solutions of D-ribose and 2-deoxy-D-ribose. *J. Phys. Chem.* **1984**, *88*, 1680-1681.

(5) Saenger, W. A Multi-Faceted Approach to Elucidate the Crystal Structure of D-Ribose: Similarities to Protein Structure Determination. *Angew. Chem. Int. Ed.* **2010**, *49*, 6487-6489.

(6) Suzuki, T.; Kawashima, H.; Kotoku, H.; Sota, T. Structural Fluctuation and Dynamics of Ribose Puckering in Aqueous Solution from First Principles. *J. Phys. Chem. B* **2005**, *109*, 12997-13005.

(7) Suzuki, T.; Sota, T. Circular Hydrogen Bond Networks on the Surface of β-Ribofuranose in Aqueous Solution. *J. Phys. Chem. B* **2005**, *109*, 12603-12611.

(8) Van Eijck, B. P.; Kroon, J. Molecular-dynamics simulations of β-d-ribose and β-d-deoxyribose solutions. *J. Mol. Struc.* **1989**, *195*, 133-146.

(9) Alkorta, I.; Popelier, P. L. A. Computational study of mutarotation in erythrose and threose. *Carbohydr. Res.* **2011**, *346*, 2933-2939.

(10) Qian, X.; Wei, X. Glucose isomerization to fructose from ab initio molecular dynamics simulations. *J. Phys. Chem. B* **2012**, *116*, 10898-10904.

(11) Molteni, C.; Parrinello, M. Glucose in aqueous solution by first principles molecular dynamics. *J. Am. Chem. Soc.* **1998**, *120*, 2168-2171.

(12) Azofra, L. M.; Alkorta, I.; Elguero, J. Theoretical study of the mutarotation of erythrose and threose: acid catalysis. *Carbohydr. Res.* **2013**, *372*, 1-8.

(13) Dejaegere, A. P.; Case, D. A. Density Functional Study of Ribose and Deoxyribose Chemical Shifts. *J. Phys. Chem. A* **1998**, *102*, 5280-5289.

(14) Jalbout, A. F.; Adamowicz, L.; Ziurys, L. M. Conformational topology of ribose: A computational study. *Chem. Phys.* **2006**, *328*, 1-7.

(15) Angyal, S. J. The composition of reducing sugars in solution: Current aspects. *Adv. Carbohydr. Chem. Biochem.* **1991**, *49*, 19-36.

(16) Mathlouthi, M.; Seuvre, A. M.; Koenig, J. L. F.T.-I.R. and laser-raman spectra of d-ribose and 2-deoxy-d-erythro-pentose ("2-deoxy-d-ribose"). *Carbohydr. Res.* **1983**, *122*, 31-47.

(17) Yaylayan, V. A.; Ismail, A. A. Investigation of the enolization and carbonyl group migration in reducing sugars by FTIR spectroscopy. *Carbohydr. Res.* **1995**, *276*, 253-265.

(18) Šišak, D.; McCusker, L. B.; Zandomeneghi, G.; Meier, B. H.; Bläser, D.; Boese, R.; Bernd Schweizer, W.; Gilmour, R.; Dunitz, J. D. The crystal structure of D-ribose - At last!. *Angew. Chem. Int. Ed.* **2010**, *49*, 4503-4505.

(19) Lemieux, R. U.; Anderson, L.; Conner, A. H. The mutarotation of 2-deoxy-β-d-erythro-pentose ("2-deoxy-β-d-ribose"). Conformations, kinetics, and equilibria. *Carbohydr. Res.* **1971**, *20*, 59-72.

(20) Tummalapalli, C. M.; Back, D. M.; Polavarapu, P. L. Fourier-transform infrared vibrational circular dichroism of simple carbohydrates. *J. Chem. Soc., Faraday Trans.* **1988**, *84*, 2585-2594.

(21) Bose, P. K.; Polavarapu, P. L. Vibrational circular dichroism of monosaccharides. *Carbohydr. Res.* **1999**, *319*, 172-183.

(22) Petrovic, A. G.; Bose, P. K.; Polavarapu, P. L. Vibrational circular dichroism of carbohydrate films formed from aqueous solutions. *Carbohydr. Res.* **2004**, *339*, 2713-2720.

(23) Taniguchi, T.; Monde, K. Vibrational circular dichroism (VCD) studies on disaccharides in the CH region: Toward discrimination of the glycosidic linkage position. *Org. Biomol. Chem.* **2007**, *5*, 1104-1110.

(24) Wen, Z. Q.; Barron, L. D.; Hecht, L. Vibrational Raman optical activity of monosaccharides. *J. Am. Chem. Soc.* **1993**, *115*, 285-292.

(25) Becke, A. D. Density-Functional Thermochemistry .3. The Role of Exact Exchange. *J. Chem. Phys.* **1993**, *98*, 5648-5652.

(26) Lee, C. T.; Yang, W. T.; Parr, R. G. Development of the Colle-Salvetti Correlation-Energy Formula into a Functional of the Electron-Density. *Phys. Rev. B* **1988**, *37*, 785-789.

(27) Frisch, M. J.; Pople, J. A.; Binkley, J. S. Self-Consistent Molecular-Orbital Methods .25. Supplementary Functions for Gaussian-Basis Sets. *J. Chem. Phys.* **1984**, *80*, 3265-3269.

(28) Tomasi, J.; Mennucci, B.; Cammi, R. Quantum Mechanical Continuum Solvation Models. *Chem. Rev.* **2005**, *105*, 2999-3094.

(29) Zhao, Y.; Truhlar, D. The M06 suite of density functionals for main group thermochemistry, thermochemical kinetics, noncovalent interactions, excited states, and transition elements: two new functionals and systematic testing of four M06-class functionals and 12 other functionals. *Theor. Chem. Acc.* **2008**, *120*, 215-241.

(30) Teklebrhan, R. B.; Owens, N. W.; Xidos, J. D.; Schreckenbach, G.; Wetmore, S. D.; Schweizer, F. Conformational Preference of Fused Carbohydrate-Templated Proline Analogues—A Computational Study. *J. Phys. Chem. B* **2012**, *117*, 199-205.

(31) Pipolo, S.; Cammi, R.; Rizzo, A.; Cappelli, C.; Mennucci, B.; Tomasi, J. Cavity field effects within a polarizable continuum model of solvation: Application to the calculation of electronic circular dichroism spectra of R-(+)-3-methyl-cyclopentanone. *Int. J. Quantum Chem.* **2011**, *111*, 826-838.

(32) Mennucci, B.; Cappelli, C.; Cammi, R.; Tomasi, J. Modeling solvent effects on chiroptical properties. *Chirality* **2011**, *23*, 717-729.

(33) Lopes Jesus, A. J.; S. F. Teixeira, M. H.; Redinha, J. S. Structure of Charged Cyclohexyldiamines in Aqueous Solution: A Theoretical and Experimental Study. *J. Phys. Chem. B* **2012**, *116*, 5019-5027.

(34) Atwood, R. E.; Urban, J. J. Conformations of the Glycine Tripeptide Analog Ac-Gly-Gly-NHMe: A Computational Study Including Aqueous Solvation Effects. *J. Phys. Chem. A* **2012**, *116*, 1396-1408.

(35) Møller, C.; Plesset, M. S. Note on an Approximation Treatment for Many-Electron Systems. *Phys. Rev.* **1934**, *46*, 618-622.

(36) Pople, J. A.; Binkley, J. S.; Seeger, R. Theoretical models incorporating electron correlation. *Int. J. Quantum Chem.* **1976**, *10*, 1-19.

(37) Pople, J. A.; Seeger, R.; Krishnan, R. Variational configuration interaction methods and comparison with perturbation theory. *Int. J. Quantum Chem.* **1977**, *12*, 149-163.

(38) Krishnan, R.; Pople, J. A. Approximate fourth-order perturbation theory of the electron correlation energy. *Int. J. Quantum Chem.* **1978**, *14*, 91-100.

(39) Frisch, M. J.; Trucks, G. W.; Schlegel, H. B.; Scuseria, G. E.; Robb, M. A.; Cheeseman, J. R.; Scalmani, G.; Barone, V.; Mennucci, B.; Petersson, G. A.; Nakatsuji, H.; Caricato, M.; Li, X.; Hratchian, H. P.; Izmaylov, A. F.; Bloino, J.; Zheng, G.; Sonnenberg, J. L.; Hada, M.; Ehara, M.; Toyota, K.; Fukuda, R.; Hasegawa, J.; Ishida, M.; Nakajima, T.; Honda, Y.; Kitao, O.; Nakai, H.; Vreven, T.; Montgomery, J., J. A.; Peralta, J. E.; Ogliaro, F.; Bearpark, M.; Heyd, J. J.; Brothers, E.; Kudin, K. N.; Staroverov, V. N.; Kobayashi, R.; Normand, J.; Raghavachari, K.; Rendell, A.; Burant, J. C.; Iyengar, S. S.; Tomasi, J.; Cossi, M.; Rega, N.; Millam, N. J.; Klene, M.; Knox, J. E.; Cross, J. B.; Bakken, V.; Adamo, C.; Jaramillo, J.; Gomperts, R.; Stratmann, R. E.; Yazyev, O.; Austin, A. J.; Cammi, R.; Pomelli, C.; Ochterski, J. W.; Martin, R. L.; Morokuma, K.; Zakrzewski, V. G.; Voth, G. A.; Salvador, P.; Dannenberg, J. J.; Dapprich, S.; Daniels, A. D.; Farkas, Ö.; Foresman, J. B.; Ortiz, J. V.; Cioslowski, J.; Fox, D. J.; Gaussian, Inc.: Wallingford CT, 2009.

(40) Cremer, D.; Pople, J. A. General definition of ring puckering coordinates. *J. Am. Chem. Soc.* **1975**, *97*, 1354-1358.

(41) Altona, C.; Sundaralingam, M. Conformational analysis of the sugar ring in nucleosides and nucleotides. New description using the concept of pseudorotation. *J. Am. Chem. Soc.* **1972**, *94*, 8205-8212.

(42) Cremer, D. Calculation of puckered rings with analytical gradients. *J. Phys. Chem.* **1990**, *94*, 5502-5509.

(43) Bader, R. F. W. *Atoms in Molecules: A Quantum Theory*; Clarendon Press: Oxford, 1990.

(44) Popelier, P. L. A. *Atoms In Molecules. An introduction*; Prentice Hall: Harlow, England, 2000.

(45) Popelier, P. L. A. A robust algorithm to locate automatically all types of critical points in the charge density and its Laplacian. *Chem. Phys. Lett.* **1994**, *228*, 160-164.

(46) Popelier, P. L. A.; 0.2 ed. 1999.

(47) Rafat, M.; Popelier, P. L. A. Visualization and integration of quantum topological atoms by spatial discretization into finite elements. *J. Comput. Chem.* **2007**, *28*, 2602-2617.

(48) Keith, T. A.; 13.02.26 ed. 2012.

(49) Cremer, D.; Kraka, E. Chemical Bonds without Bonding Electron Density — Does the Difference Electron-Density Analysis Suffice for a Description of the Chemical Bond?. *Angew. Chem. Int. Ed.* **1984**, *23*, 627-628.

(50) Rozas, I.; Alkorta, I.; Elguero, J. Behavior of Ylides Containing N, O, and C Atoms as Hydrogen Bond Acceptors. *J. Am. Chem. Soc.* **2000**, *122*, 11154-11161.

(51) Weinhold, F.; Landis, C. R. *Valency and Bonding. A Natural Bond Orbital Donor- Aceptor Perspective*; Cambridge Press: Cambridge, 2005.

(52) Glendening, E. D.; Reed, A. E.; Carpenter, J. E.; Weinhold, F. NBO 3.0, Theoretical Chemistry Institute, University of Wisconsin, Madison, 2001.

(53) http://vicinv.ujaen.es/sti_cict.

(54) Real Crystal® IR sample cards. U.S. Patent No. 7, 095 & UK Patent No. GB2372102.

(55) Kuroda, R.; Harada, T.; Shindo, Y. A solid-state dedicated circular dichroism spectrophotometer: Development and application. *Rev. Sci. Instrum.* **2001**, *72*, 3802-3810.

(56) Merten, C.; Kowalik, T.; Hartwig, A. Vibrational circular dichroism spectroscopy of solid polymer films: Effects of sample orientation. *Applied Spectroscopy* **2008**, *62*, 901-905.

(57) Buffeteau, T.; Lagugné-Labarthet, F.; Sourisseau, C. Vibrational circular dichroism in general anisotropic thin solid films: Measurement and theoretical approach. *Applied Spectroscopy* **2005**, *59*, 732-745.

(58) Barnett, C. B.; Naidoo, K. J. Ring Puckering: A Metric for Evaluating the Accuracy of AM1, PM3, PM3CARB-1, and SCC-DFTB Carbohydrate QM/MM Simulations. *J. Phys. Chem. B* **2010**, *114*, 17142-17154.

(59) Dowd, M. K.; French, A. D.; Reilly, P. J. MM3 Modeling of Ribose and 2-Deoxyribose Ring Puckering. *J. Carbohydrate Chem.* **2000**, *19*, 1091-1114.

(60) Steinmann, S. N.; Piemontesi, C.; Delachat, A.; Corminboeuf, C. Why are the Interaction Energies of Charge-Transfer Complexes Challenging for DFT?. *J. Chem. Theory Comput.* **2012**, *8*, 1629-1640.

(61) Solimannejad, M.; Massahi, S.; Alkorta, I. Glyoxal oligomers: A computational study. *Int. J. Quantum Chem.* **2011**, *111*, 3057-3069.

(62) Mata, I.; Alkorta, I.; Molins, E.; Espinosa, E. Universal Features of the Electron Density Distribution in Hydrogen-Bonding Regions: A Comprehensive Study Involving H···X (X=H, C, N, O, F, S, Cl, π) Interactions. *Chem. Eur. J.* **2010**, *16*, 2442-2452.

(63) Alkorta, I.; Rozas, I.; Elguero, J. Bond Length–Electron Density Relationships: From Covalent Bonds to Hydrogen Bond Interactions. *Struct. Chem.* **1998**, *9*, 243-247.

(64) Bender, M. L.; Brubacher, J. L. *Catálisis y acción enzimática;* Reverté, Spain, 1977.

(65) Voet, D.; Voet, J. G. *Bioquímica* 3ª Edición; Editorial médica Panamericana, Buenos Aires, 2006.

(66) Yang, G.; Pidko, E. A.; Hensen, E. J. M. Mechanism of Bronsted acid-catalyzed conversion of carbohydrates *J. Catal.* **2012**, *295*, 122-132.

(67) Lemieux, R. U.; Hendriks, K. B.; Stick, R. V.; James, K. Halide ion catalyzed glycosidation reactions. Syntheses of .alpha.-linked disaccharides *J. Am. Chem. Soc.* **1975**, *97*, 4056-4062.

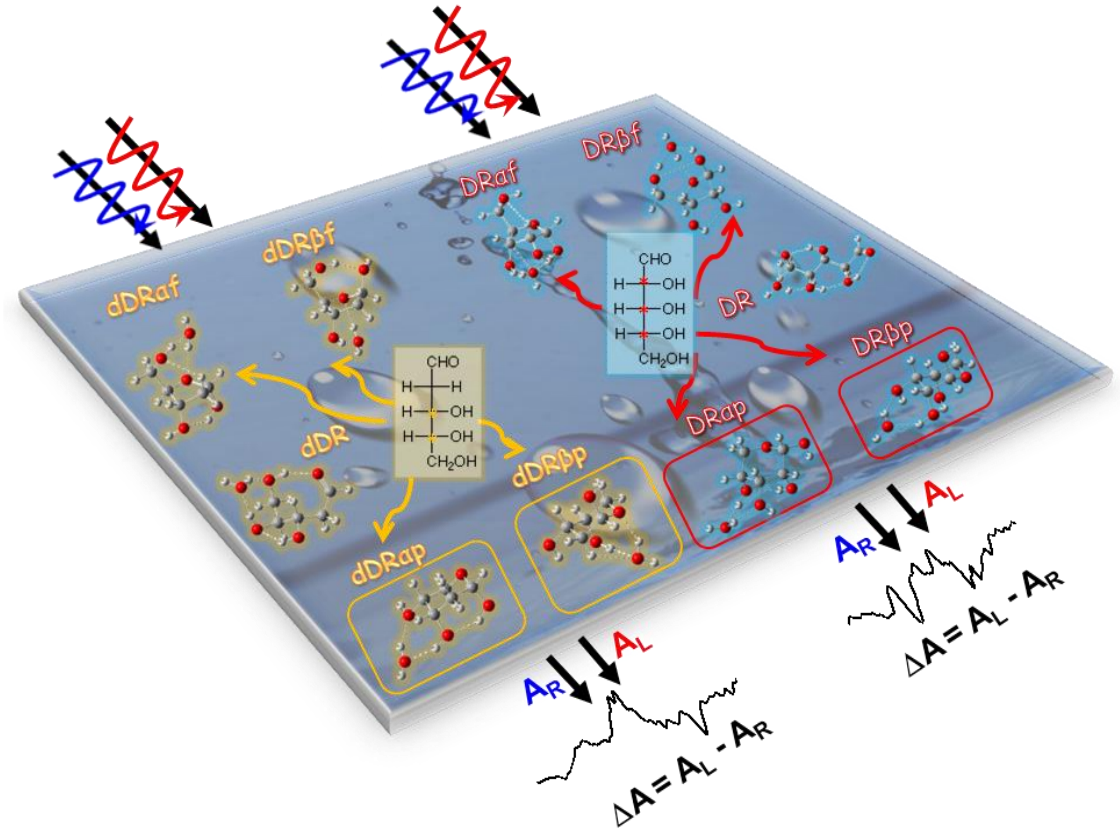
DRαf
DRβf
dDRαf
dDRβf
CHO
H—OH
H—OH
H—OH
CH2OH
DR
DRβp
DRαp
dDR
dDRβp
dDRαp
AL
AR
ΔA = AL - AR